Development of Image Analysis Methods for Flowing Soap Films as a Two-Dimensional Turbulence and Analysis of the Effects of Polyethylene Oxide on the Flow

2010. 9

Biochemistry and Biotechnology

United Graduate School of Agricultural Science

Tokyo University of Agriculture and Technology

HIDEMA Ruri

（日出間るり）

Contents

Chapter 1

General Introduction

1.1. Overview

Fluid mechanics consist of fluid dynamics and fluid statics, which has a very long history. The study of fluid mechanics goes back at least to the days of ancient Greece, and we can see a lot of great physicist and mathematician. One of the noblest consequences is that the Navier-Stokes equations which describe the motion of fluid substances. While it is possible to find some particular solutions of the Navier-Stokes equations governing fluid motion, all such solutions are unstable at large Reynolds numbers, namely, turbulence. Sensitive dependence on the initial and boundary conditions makes fluid flow irregular both in time and in space that is why a statistical description is needed. Andrey Kolmogorov proposed the first statistical theory of turbulence, based on the energy cascade (an idea originally introduced by Lewis Fry Richardson) and the concept of self-similarity [1,2]. This statistical theory of turbulence, that is, the scaling method is still useful technique to describe the flow.

An attempt to solve the Navier-Stokes equations numerically was also started in the 1930s. At the first stage, the calculation was applied to an airfoil from the two-dimensional point of view. In the 1960s, the computer power became available to make three-dimensional calculation. The computational fluid dynamics is developing with the development of the computer, which allows scientists to visualize the turbulence even in very small scale. However, to describe the flow completely by numerical simulation is still difficult, since the theory and experiment are always little different. This is the reason why a new current to study the flow more experimentally is needed, which is the particle image velocimetry (PIV). The PIV technique makes it possible to describe the flow field [3]. In order to see the flow field simpler, the study of two-dimensional turbulence has also been developed. Flowing soap films are one of the techniques to make 2D flow in laboratories [4]. Soap films make the interference patterns on the film by reflecting the illumination light, which is related to the thickness of the film. That is why, the interference pattern of the soap film includes the instantaneous thickness information, furthermore the instantaneous flow information on the film.

Since the turbulence is the most complicated, the most troublesome and the most common flow in fluids dynamics, the turbulence have been discussed in various areas, and the turbulence was tried to be inhibited in industries. For instance, it is known that minute amounts (20-30ppm) of

long chain molecules reduce the drag force in turbulences, which is called drag reduction [1-3]. This phenomenon is used to improve energy efficiency. Therefore, applications of drag reduction can be found in various industrial areas such as the transport of crude oil, increasing volumetric flow rate of water in fire fighting and so on [5,6]. This phenomenon was investigated by Toms [7], and the mechanism of this effect has been a long-standing issue. The interaction between the polymer and the walls of the container, or the interaction between the turbulent flow itself and the long chain molecules are the main problem for the mechanism of the drag reduction [8]. The first explanation of the drag reduction is made by Lumley, which indicates that the polymer chains may stretch in the outside of the viscous sublayer if the strain rate in the turbulence are sufficiently large, while polymer chain cannot be extended in the viscous sublayer. This stretching and compressing effects on the polymer chain will reduce the velocity gradient at the wall, and so reduce the drag [9, 10]. In Lumley's theory the presence of walls plays a major role. However it is indicated that the drag reduction can occur in far away from the walls. This fact led de Gennes and Tabor to speculate on a different way to explain the drag reduction phenomena by considering the polymer dynamics. In the de Gennes-Tabor scenario the polymers store up energy in turbulent flow, and so the drag reduction can be occurred [11]. In recent, the current of Lumley investigated that the stabilization of the buffer layer of the turbulent is important for the drag reduction (Fig. 1.1) [12]. The current of de Gennes and Tabor shows that polymers are coiled up into very small balls, while they may stretch considerably under the flow (Fig. 1.2) [13]. An elongational viscosity will be large in these flows, and the elastic modulus of the polymer solution will be important in these flows [14]. At least, the coil and stretch transition under the turbulence is important for the drag reduction, thus, only the long flexible polymer such as polyethylene oxide can make drag reduction. As mentioned here, the mechanism of drag reduction is still extensive studies, however a complete explanation for the phenomenon has not been reported.

In order to approach the drag reduction effects simpler, turbulence on flowing soap films is also useful. Since flowing soap films show the flow information by reflecting the illumination light, the variation of the turbulence by polymer additives can easily be seen on the interference pattern of the film. The flowing soap films are made by surfactant bilayer, thus the polymer is inside the sandwich structure of the bilayer (Fig. 1.3). Such situations include not only the problem of the effect of polymer in 2D turbulence but also the topic of the interaction between surfactants and

polymer, or polymer and polymer in confined reaction space. Indeed, such a confined complex system can be seen in various areas. For instance, the cell membranes are made by surfactant bilayer contains proteins (Fig. 1.4)[15]. Synovial fluid is also non-Newtonian very thin 2D fluids, 50 μm, which contains biological polymer like a hyaluronic acid (Fig. 1.5)[16]. These cell membrane and synovial fluids can keep the inside water in laminar flow state, even under the sudden external forces. This effect inhibits the increase of frictional force in these areas. Thus, the investigation of effects of polymer in flowing soap films has a full of probability to consider not only fluids dynamics but also biology which is familiar to our life.

The aim of this thesis is to propose a new analysis technique and ideas in order to analyze turbulence. Interference patterns of the flowing soap films as a 2D turbulence are used for this analysis, since the interference pattern visualize the flow information easily as described before. This new method is named as IFI methods, that is, *i*nter*f*erence *i*mage analysis. IFI method let the turbulent analysis much easier and makes it possible to see broad area than previous work. Besides, polyethylene oxide as a polymer was added to the turbulence in order to quantify the variation of the turbulence by the IFI method. Indeed, this method could detect the effects of polyethylene oxide on the turbulence. This original way of analysis gives a new observation technique to investigate turbulence and drag reduction but also to other complex systems in various areas such as cell membrane or synovial fluid. The brief overview is listed at the following.

This thesis consists of four chapters.

In this chapter, the over view of this thesis, brief history and analyses of the fluid dynamics, several discussion of drag reduction, what are 2D fluids and several 2D flows in nature are introduced.

In chapter 2, the theoretical backgrounds of this thesis are explained. General explanation of the effect of polymer in turbulence, important features of 2D turbulence and the general analytical method of 2D turbulence are in this chapter.

In chapter 3, 2D turbulence on flowing soap films were visualized by the interference pattern, besides these interference patterns were analyzed by single-image analysis which is called IFI method. IFI method includes three types of analyses, that is, Fourier transformation method,

Curvature analysis method and Color distribution analysis method [17]. Fourier transformation method quantifies the thickness fluctuations of turbulent soap film by the power spectrum of the interference patterns. Curvature analysis method calculated the curvatures of the interference pattern of turbulent soap films. The curvature histogram is related to the distribution of the velocity fluctuations. The velocity fluctuations are also discussed by the Color distribution analysis, which is derived by the color intensity of the interference image. Polyethylene oxide was added in order to see the variation of the turbulence. Beside, this variation is visualized and analyses by the IFI method. Indeed, the effects of polyethylene oxide on the flowing soap films turbulence as a 2D turbulence is described well by the IFI method.

In chapter 4, we briefly summarize all of the discussion in this thesis. The possible applications of this research are discussed.

1.2. Reference

[1] A. N. Kolmogorov, Local structure of turbulence in an incompressible fluid for very large Reynolds numbers, *Doklady Acad Sci. USSR.* **31**, 301 (1941)

[2] S. Kida, S. Yanase, Turbulence dynamics, Asakura Publishing Company (1991)

[3] J. Westerweel, Digital particle image velocimetry - Theory and application, Delft University Press (1993)

[4] H. Kellay, W. I. Goldburg, Two-dimensional turbulence: a review of some recent experiments, *Rep. Prog. Phys.* **65**, 845 (2002)

[5] C. A. Kim, J. H. Sung, H. J. Choi, C. B. Kim, W. Chun, M. S. Jhon, Drag Reduction and Mechanical Degradation of Poly(ethylene oxide) in Seawater, *J. Chem. Eng. Jap.* **32**, 803 (1999)

[6] J. F. Motier, L. C. Chou, J. R. Harris, N. Kommareddi, Polymer Advances and the Dramatic Growth in Commercial Pipeline Drag Reduction, 12th European Drag Reduction Meeting (2002).

[7] B. A. Toms, in Proceedings of the International Congress on Rheology, North Holland, Amsterdam (1949)

[8] K. R. Sreenivasan, C. M. White, The onset of drag reduction by dilute polymer additives, and the maximum drag reduction asymptote, *J. Fluid. Mech.* **409**, 149 (2000)

[9] G. Ryskin, Turbulent Drag Reduction by Polymers: A Quantitative Theory, *Phys. Rev. Lett.* **59**, 2059 (1987)

[10] J. L. Lumley, Drag reduction in turbulent flow by polymer additives, *J. Polym. Sci: Macromol Rev.* **7**, 263 (1973)

[11] D. Thirumalai, J. K. Bhattacharjee, Polymer-induced drag reduction in turbulent flows, *Phys. Rev.E.* **53**, 546 (1996)

[12] R. Benzi, E. De Angelis, V. S. L'vov, I. Procaccia, Identification and Calculation of the Universal Asymptote for Drag Reduction by Polymers inWall Bounded Turbulence, *Phys. Rev. Lett.* **95**, 194502 (2005)

[13] D. E. Smith, S. Chu, Response of Flexible Polymers to a Sudden Elongational Flow, *Science*, **281**, 1335 (1998)

[14] G. Boffetta, A. Celani, S. Musacchio, Two-dimensional turbulence of dilute polymer solutions, *Phys. Rev. Lett.* **91**, 034501 (2003)

[15] NIST Center for Neutron Research, http://www.ncnr.nist.gov/programs/reflect/rp/biology/cell_membrane.html

[16] http://en.wikipedia.org/wiki/Joint

[17] R. Hidema, Z. Yatabe, M. Shoji, C. Hashimoto, R. Pansu, G. Sagarzazu, H. Ushiki, Image analysis of thickness in flowing soap films. I: effects of polymer, *Exp. Fluids*, in press (2010)

(a)

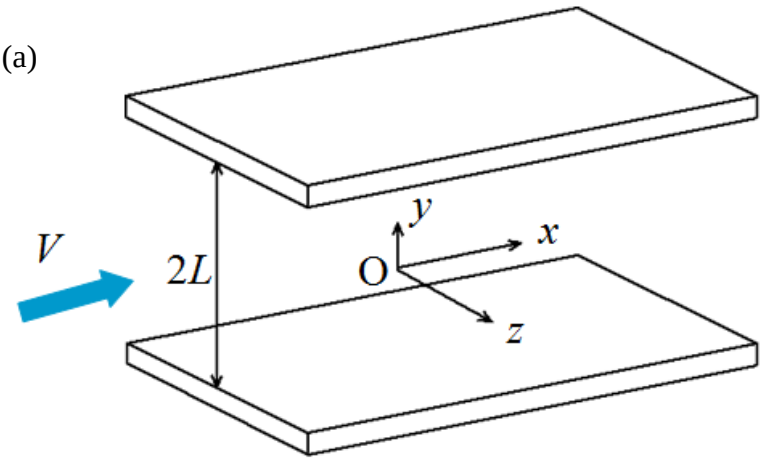

(b)

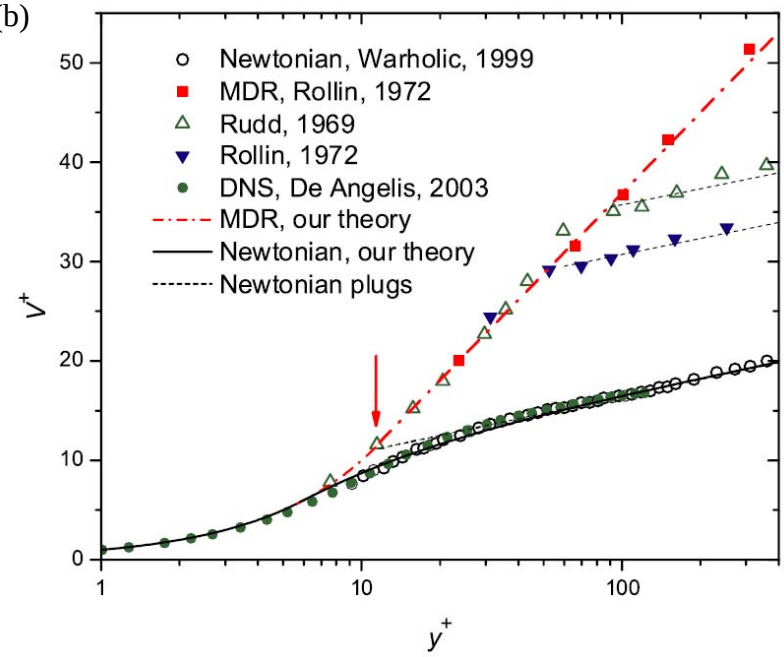

Figure. 1.1(a). Schematic of the flow in two plates. V is the mean velocity, $2L$ is the distance of the two plates, x, y, and z are the streamwise, wall-normal, and spanwise directions, respectively.

(b) Mean normalized velocity profiles as a function of the normalized distance from the wall, that is, $V^+(y^+)$ which is in the x direction with a dependence on y only [12]. To be precise, $V^+ \equiv V/\sqrt{p'L}$ where p' is the fixed pressure gradient $-\partial p/\partial x$ and L is the midheight of the channel, $y^+ \equiv y\,\mathrm{Re}/L$ where Reynolds number is $\mathrm{Re} \equiv L/\sqrt{p'L}/\nu_0$. Near the wall, Newtonian flow (○, ●, —, ---) follow the viscous sublayer where the velocity is proportionally increase from the wall. The velocity profile is turned to the log law region. Polymer additives change the transition region (■, △, ▼, ---).

(a)

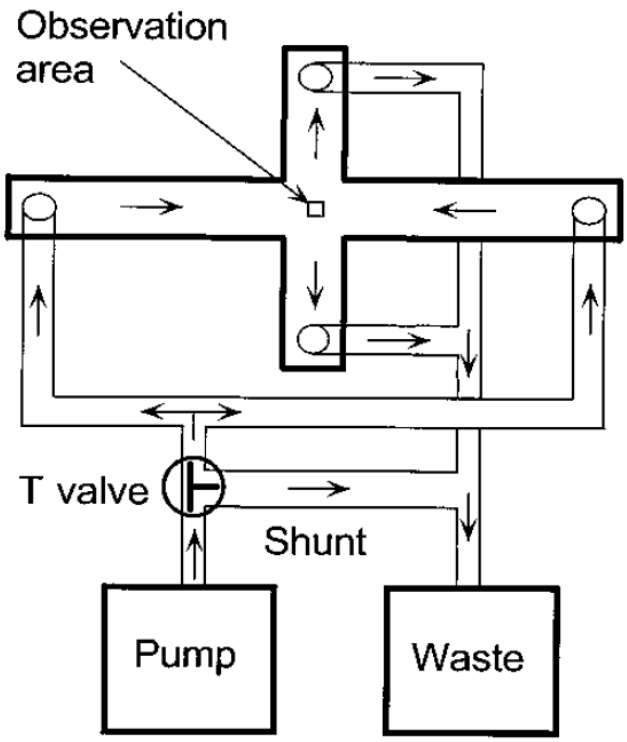

(b)

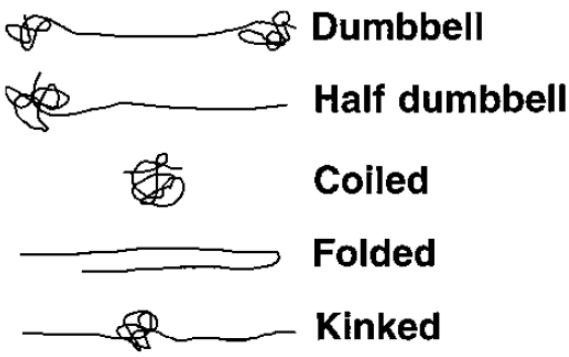

Figure. 1.2. (a) is the schematic diagram of a apparatus which detect the polymer stretching under the flow [13]. Fluorescently labeled DNA molecules (λ-DNA, $L_{strained} \cong 22$ μm) as long chain polymers are put under the observation area and elongational flow at $\dot{\varepsilon} = 0.86\text{s}^{-1}$ are made suddenly by the apparatus. $\dot{\varepsilon} \approx \frac{0.5}{\tau_1}$ where τ_1 is longest relaxation time of the polymer. Polymers are at least stretched under the turbulence, as shown in (b).

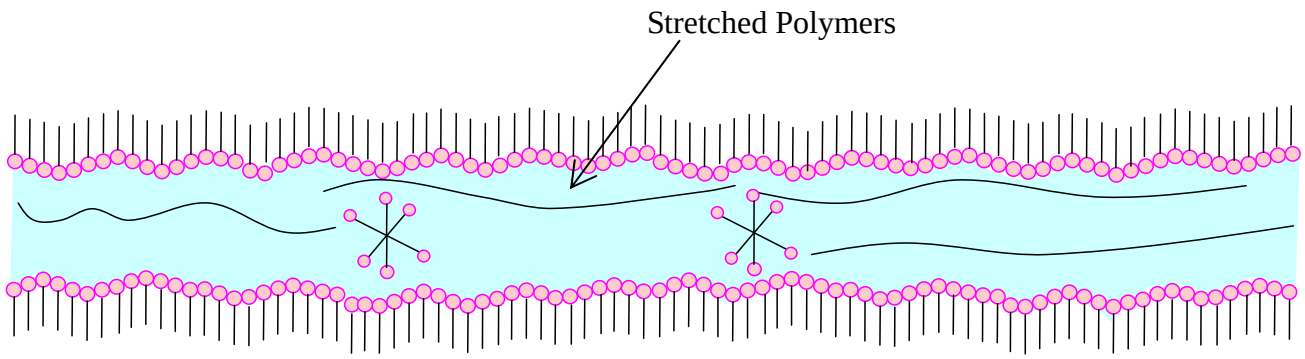

Figure. 1.3. Cross section diagram of the soap films. Polymers are stretched under the 2D turbulence made by surfactant bilayer.

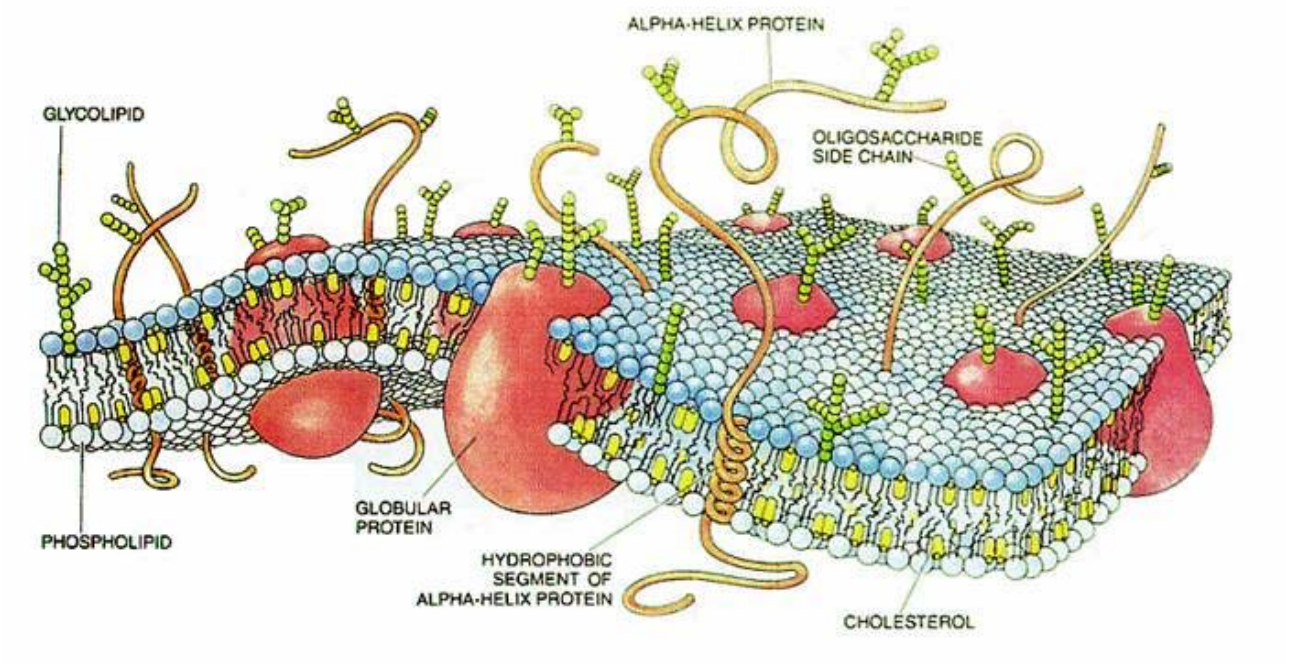

Figure. 1.4. Schematic of cell membranes that is made by surfactant bilayer contains proteins [15].

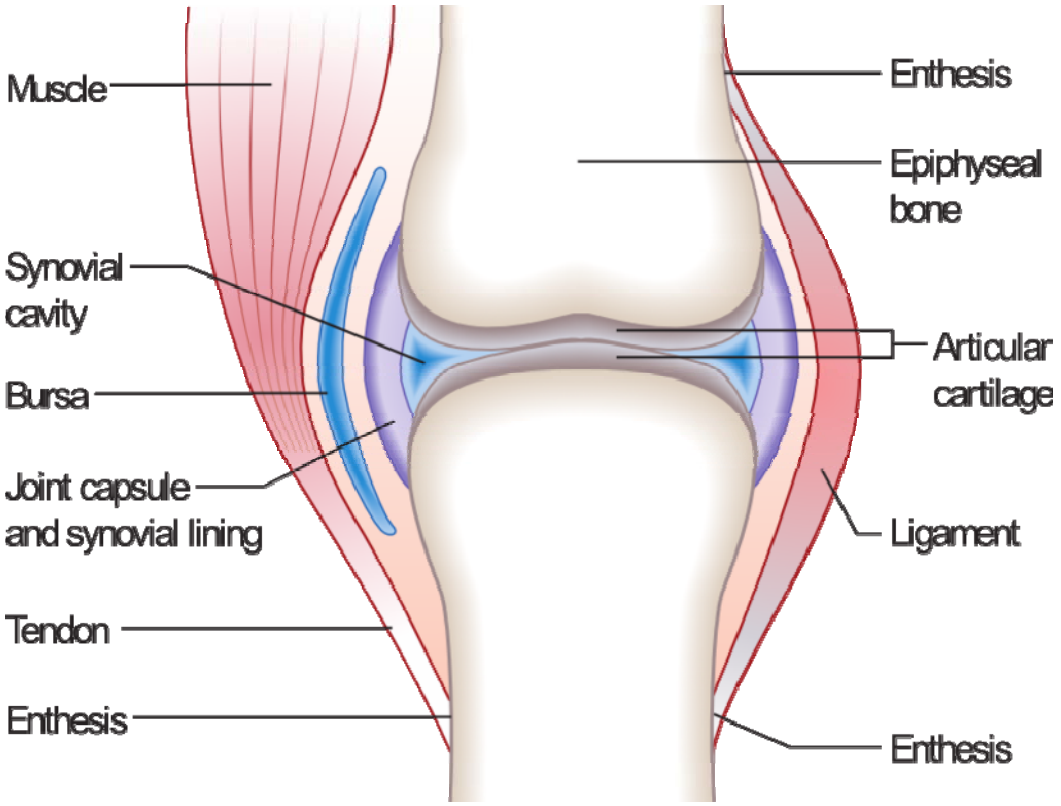

Figure. 1.5. Schematic of joint of the human body. Synovial fluid is non-Newtonian very thin 2D fluids, 50 μm [16].

Chapter 2

Theoretical Background of Two-dimensional Turbulence and Effects of Polymer

2.1. Abstract

Two-dimensional turbulence is different from three-dimensional turbulence caused by absence of the vortex stretching. This feature derives the inverse energy cascade and the conservation of the enstrophy, namely, enstrophy cascade. In 2D turbulence, the energy is dissipated in larger scale by friction. Small amounts of polymer affect the inverse energy cascade, thus, the energy dissipation in larger scale is decreased. This phenomenon is called *friction reduction*. On the other hand, the enstrophy cascade is hardly affected by polymer additives. These characteristic of 2D turbulence are explained by the scaling law of the fluid dynamics. Besides, a distribution function that can describe velocity fluctuations is proposed.

2.2. Introduction

Historically, two-dimensional turbulence was the province of the theorist and the scientist who want to solve the Navier-Stokes equation numerically. Also, the meteorologists and oceanographers use the ideas of 2D flow, since the turbulence in the air such as typhoon or in the oceans such as waves are approximately 2D. From the latter 1990s, the experiment of flowing soap films is becoming familiar in fluid dynamic laboratories. In the first stage, the flowing soap films were just useful for visualization and calculation. After the first attempt to observe the soap film, characteristics of 2D flow have also been observed, such as the inverse energy cascade and enstrophy cascade caused by the absence of the vortex stretching. These cascade shows the scaling law, the scaling exponent are affected by polymer additives.

In this chapter, the theoretical back ground of the 2D flows and effects of polymers are explained.

2.3. Two-dimensional turbulence

2.3.1. Soap films as a two dimensional turbulence [1, 2]

Soap films have been intrigued by many great historical scientists, and much has been published about them. The standard view of a soap membrane is a micrometer thick sheet of water covered on either side by surfactant molecules. Without the surfactant the liquid sheet would be unstable and break up into droplets. Surfactants endow the film with elasticity, or restoring force, against any local thinning that could lead to rupture. The basic picture of a cross section of a soap film attached to rigid supports is sketched in Fig. 2.1. For a soluble surfactant can reside both on the surface and inside the interstitial fluid sheet. If the soap concentration exceeds the critical micelle concentration, the interior of the film will also contain spherical or cylindrical micelle structures (Fig. 2.1.a). These dissolved molecules can replenish the surface when the film is stretched slowly. The soap films contain typically 98 or 99% water and 1 or 2 % commercial detergent or a pure surfactant. Soap film can stretch in its area 10^4 or 10^5 times wider than its thickness. That is why the soap film can be considered as 2D flow. Soap films reflect the illumination light in the front and back surfaces of the film, thus the film exhibit colors due to optical interference. Therefore, soap films provide a natural way to visualize the 2D flow caused by thickness fluctuations (Fig. 2.1.a).

2.3.2. History of two-dimensional turbulence

The first experimental work of soap films in a laboratory was given by Couder in the beginning of the 1980s [3, 4]. They used two rectangular frames of length 33 cm, 10.6 and 15.8 width respectively. In order to make the soap film, the rectangular frames were dipped in the soap solution, then, after a very short drainage, set in a horizontal position. There was a strong thickness gradient near the frame then a slowly varying thickness (from 10 μm to 12 μm) in the central area 12 cm wide. Couder towed a cylinder through a soap film and could take a photograph of the von Karman street (Fig. 2.2.a, b). The images are taken in reflection using monochromatic light. In order to produce an initially turbulent flow, Couder towed a grid formed from an array of cylinders 0.2 cm in diameter with a spacing of 0.1 or 0.2 cm between the cylinders (Fig. 2.2.c). The towing

speed was ranging from 5 cm/s to 60 cm/s. Findings on the stability of Karman vortex streets, and the coarsening of vortices in 2D turbulence were reported in his work [1, 3].

As a next step of the soap film experiments, Gharib and Derango [5, 6] built a device where the film flows down a channel, more like a conventional wind tunnel. They made a soap film from a solution reservoir, along rigid rails, and onto a sheet of rapidly moving pure water (Fig. 2.3.a). With this technique, they eliminated the short observation period and non-uniform film thickness problems from the 2D flow. The flow of the water sheet and the surface tension difference between the pure water and the soapy film drives the film forward. This surface tension difference limits the maximum speed of the film to about 30 cm/s at a film thickness of about 6 μm, which was observed by using a laser Doppler velocimetry. Various types of the flow were observed on the 2D flow, which was twin vortex, Karman vortex, turbulence, and so on. Even with this early stage of the 2D flow experiments, power spectra of the velocity fluctuation in turbulence were calculated, which followed the scaling property predicted by Kraichinan and Batchelor [5, 7-9].

Kelley et al. developed a flowing film method as shown in Fig. 2.3.b [12]. The soap film channel was driven by gravity and fed by a reservoir which was filled with soap solution. The film spanned a pair of parallel vertical wires of separation 5 cm that were attached to the reservoir floor. The soap solution in the reservoir was fed into the film by small holes, of radius 0.02 cm, drilled into the reservoir bottom. The wires were weighted at the bottom end, and these weights were suspended in a second reservoir also filled with soap solution. The length of the wires was 180 cm. The film thickness was 5 μm, and the mean vertical film speed could be varied between 20 cm/s to 4 m/s.

Rutgers et al. [2] established the 2D flowing soap film system in the late 1990s. The new apparatus is shown in Fig. 2.4. The fluid element starts in the upper supply reservoir (a) where it is driven downward into the feed tube (b) by a pressure head ΔP. A fluid metering valve (c) sets the flow rate. The feed tube is connected to the top of a nozzle (d). Two monofilament nylon guide wires (e) disappear into the bottom of the nozzle. Thinner nylon pull lines (f) are attached to the guide wires and hold them apart. As the fluid element is ejected from the nozzle, it stretches between the guide wires as it is accelerated by gravity in the expansion section (I) of the channel. The element rapidly gains area due to vertical (y) and horizontal (x) stretc hing and air drag slows it from its free fall trajectory. In the test section (II) the guide wires are parallel and the fluid element

has reached a near constant "terminal velocity" due to the balance between gravitational and air drag forces. During this time the soap film is between 2 and 6 micrometers thick and travels between 0.5 and 4 m/s, depending on the fluid injection rate. At the bottom of the channel the element encounters the contraction section (III) where the film thickens and slows in a process nearly the reverse of the expansion section (I). The film finally drips from the guide wire tensioning weight (g) in to the bottom collection reservoir (h). With the new apparatus, the 2D flow field can have uniform thick and very high speed. Now, many 2D flow researches follow this new apparatus.

2.3.3. Features of 2D turbulence in the definition of vortex stretching, energy and enstrophy [1]

There is general agreement that all the flow properties of Newtonian fluids in two or three dimensions are encompassed in the Navier-Stokes equation for the velocity $\mathbf{v}(x,t)$:

$$\mathbf{D}\mathbf{v}/\mathbf{D}t \equiv \partial\mathbf{v}/\partial t + (\mathbf{v}\bullet\nabla)\mathbf{v} = -\nabla p/\rho + \nu\nabla^2\mathbf{v}, \tag{2.1}$$

where $\mathbf{D}\boldsymbol{g}/\mathbf{D}t$ is called the convective derivative of the vector function $\boldsymbol{g}$. Here ρ is the density of the fluid, ν is its kinematic viscosity and p is the pressure. It is assumed here that the fluid is incompressible, i.e. $\nabla\bullet\mathbf{v} = 0$. The difference between 2D and 3D flows is not apparent from this equation, but the difference will appear if we consider an equation for the vorticity $\omega = \nabla\times\mathbf{v}$ of an incompressible fluid. For each component, i, of $\boldsymbol{\omega}$ and $\mathbf{v}$

$$\mathbf{D}\boldsymbol{\omega}_i/\mathbf{D}t \equiv (\boldsymbol{\omega}\bullet\nabla)\mathbf{v}_i + \nu\nabla^2\boldsymbol{\omega}_i. \tag{2.2}$$

Here, if we consider the special case where, at a certain instant of time, $\boldsymbol{\omega} = (0,0,\omega_z)$, with the viscous damping term being small. Then $\mathbf{D}\omega_z/\mathbf{D}t = \omega_z\partial u_z/\partial z$. If $\partial u_z/\partial z > 0$, ω_z will momentarily commence growing at an exponential rate. Clearly the vorticity is not a conserved quantity in 3D. It can be magnified by appropriately oriented velocity gradients. As an example, we can imagine water circulating as it flows downward through a funnel. By conservation of angular momentum, the flow will pick up angular speed as it proceeds downward through the contraction, so that the magnitude of the vorticity is increased in the direction of the velocity gradient. This amplification effect is called vortex stretching.

Vortex stretching is absent in two dimensions, because the velocity gradient is always perpendicular to the vorticity, which is necessarily perpendicular to the plane of motion. Hence the

first term on the right in Eq. (2.2) is absent, assuring that for an inviscid fluid

$$\mathbf{D}\omega / \mathbf{D}t = 0 \tag{2.3}$$

if forcing is absent. Indeed, $\omega(\mathbf{r},t)$ can change locally, but its mean value averaged over the sample area A

$$Z = (1/A)\int \omega^2 \mathbf{d}^2\mathbf{r} \tag{2.4}$$

is a constant of the motion, as are all other vorticity moments. This quantity is called the enstrophy.

In this same inviscid limit, the kinetic energy of the fluid per unit mass ε in any number of dimensions is conserved:

$$\varepsilon = (1/A)\frac{1}{2}\int v^2 \mathbf{d}^2\mathbf{r} \tag{2.5}$$

In a real fluid, where the kinetic energy of the flow is ultimately converted into heat through the viscosity term in Eq. (2.1), one must continuously inject energy (and enstrophy for 2D system) if the turbulent fluid is to be kept in a steady state. The energy and enstrophy injection rate ϵ and β are, respectively,

$$\epsilon = -\mathbf{d}\varepsilon / \mathbf{d}t \tag{2.6}$$

and

$$\beta = -\mathbf{d}Z / \mathbf{d}t \tag{2.7}$$

The enstrophy injection rate is interest only in two dimensions. The strength of the nonlinear term in Eq. (2.1) in 2D and 3D turbulence is governed by the ratio of the convective derivative term to the dissipative term. From dimensional considerations, this ratio, called the Reynolds number *Re*, has the form

$$Re = UL/\nu \tag{2.8}$$

where U and L are characteristic velocities and lengths in the turbulent system, respectively. For example, U might be taken to be the mean flow speed or the rms velocity fluctuations $\mathrm{v}_{\mathrm{rms}}$ of the turbulent flow, and L might be an aperture size of a grid in 2D or 3D turbulence. Quite often L is taken to be the 'Taylor microscale' λ, which is often defined as

$$\lambda = \mathrm{v}_{\mathrm{rms}} / \sqrt{\left\langle \partial \mathrm{v}_x / \partial x \right|^2 \rangle} \tag{2.9}$$

with x taken as the direction of the mean flow. A flow is said to be appreciably turbulent when the Reynolds number Re_λ is more than 100. The brackets denote a statistical average or, where

appropriate, a time average.

2.3.4. Velocity spectra [1]

Decomposing the velocity field in d dimensions into its spatial Fourier components, one has

$$\mathbf{v}(\mathbf{k},t) = (1/2\pi)^d \int_{-\infty}^{\infty} \mathrm{v}(\mathbf{r},t) \mathrm{e}^{-\mathrm{i}k \bullet r} \mathbf{dr} \tag{2.10}$$

The nonlinear term in the Navier-Stokes equation couples velocity fluctuations of wave number **k**. The most interesting thing is that the energy density per unit wave number per unit mass, $E(k)$, for homogeneous and isotropic turbulence. This quantity is defined so that

$$\varepsilon = \frac{1}{2}\langle \mathbf{v}^2 \rangle = \int_0^{\infty} E(k) dk \tag{2.11}$$

where $k = \sqrt{\mathbf{k}^2}$ is the magnitude of a vector in two or three dimensions. In all dimensions, $E(k)$ has units of m^3s^{-2}. Invoking the Wiener-Khinchine theorem, one can show that $E(k)$ is proportional to the Fourier transform of $\langle \mathbf{v}(x) \bullet \mathbf{v}(x+\mathbf{r}) \rangle$, where both velocity components are measured at the same time t.

From dimensional arguments or the cascade picture it follows that, in 2D or 3D,

$$E(k) = \text{const} \in^{2/3} k^{-5/3} \qquad k_d < k < k_{\text{inj}} \tag{2.12}$$

where $k_d = 1/r_d$, $k_{\text{inj}} = 1/r_{\text{inj}}$. r_d is the dissipative range. r_{inj} is the injection scale.

In 3D experiments, there is much evidence to support this *five-thirds law* in the inertial range. In most experiments, $E(k)$ is extracted from a measurement of the longitudinal x and x+**r** being two co-linear points in the direction of the mean flow. In 2D, where only a few spectral measurement have been made (because, the scaling -5/3 can occur only in forced 2D turbulence), the Wiener-Kinchine theorem, applied to isotropic turbulence, gives

$$E(k) = A \int_0^{\infty} [C(x) \cos kx] dx \tag{2.13}$$

where A=1/π to ensure that $\int_0^{\infty} E(k) dk = \langle \mathbf{v}^2 \rangle$.

In the enstrophy range, dimensional considerations dictate that, in 2D,

$$E(k) = \text{const}\beta^{2/3}k^{-3} \qquad k_{\text{inj}} < k < k_d \tag{2.14}$$

if $E(k)$ is to vary as a power of k. In the dissipative range, $k < k_d = \left(\beta / \nu^3\right)^{1/6}$.

The power component -5/3 and -3 are useful to see the inverse energy cascade and the enstrophy cascade in 2D. Inverse energy cascade is typically for 2D turbulence, that is, the energy transfers from small scale to large scale in the flow. That is why the -5/3 can be seen in larger scale in 2D, which was suggested by Kraichinan [7]. The advection of the energy can be observed by the scaling of the longitudinal nth moment in 2D, which is defined as

$$S_n = \left\langle \left(\mathbf{v}(x+\mathbf{r}) - \mathbf{v}(x) \bullet \mathbf{r}/r\right)^n \right\rangle \equiv \left\langle \delta v(r)^n \right\rangle. \tag{2.15}$$

2.3.5. Analytical method for flowing soap films

Until rather recently, flowing soap films experimental studies usually involved single-point measurements of the flow via laser Doppler velocimetry (LDV), and this technique is still very important. The time series of the velocity fluctuations in a single-point can be observed with this technique, and then the data is analyzed by Fourier transformation. Many experiments have been made in order to confirm the scaling law for each physical value in the inverse energy and enstrophy cascade ranges [1,10,11, 12-19]. And also, some kinds of probability density function, such as, velocity fluctuations and enstrophy flux, are discussed [11, 20]. Thickness fluctuations also can be measured by using LDV. The mean thickness is estimated from the relation

$$h = Q/VW \tag{2.16}$$

where Q is the flux of the flow, V is the mean velocity as measured by LDV, and W is the channel width of the flowing soap films (Fig. 2.4). Thickness fluctuations are also used in order to confirm the scaling law, and are also used in order to discuss probability density function [10, 11, 19].

However the single-point measurement is useful, this technique has a difficulty to measure *flow field*. Kellay et al. [13] reported vorticity fluctuations by using two points measurement on decaying flowing soap films (Fig. 2.5). Vorticity is constructed from the measured velocity in two different locations. Both components of the velocity are needed at different positions simultaneously,

since the vorticity is given by

$$\omega = d\mathrm{v}_y / dx - d\mathrm{v}_x / dy \tag{2.17}$$

where v_x and v_y are, respectively, the transverse and longitudinal components of the velocity. The other derivative term is constructed using the frozen turbulence assumption. The transverse component is measured at time t and time $t+\Delta t$ such that $\overline{V}\Delta t = \Delta y = \Delta x$ and the spatial derivative $d\mathrm{v}_x / dy$ is taken as $\left[\mathrm{v}_x(t+\Delta t) - \mathrm{v}_x(t)\right] = \overline{V}\Delta t$. Denoting the four velocities, two for each point are recorded as $(\mathrm{v}_{x1}, \mathrm{v}_{y1})$ and $(\mathrm{v}_{x2}, \mathrm{v}_{y2})$ the vorticity is evaluated as

$$\omega = \frac{1}{2}\left[\mathrm{v}_{y2}(t) - \mathrm{v}_{y1}(t) + \mathrm{v}_{y2}(t+\Delta t) - \mathrm{v}_{y1}(t+\Delta t)\right]/\Delta x - \frac{1}{2}\left[\mathrm{v}_{x1}(t+\Delta t) - \mathrm{v}_{x1}(t) + \mathrm{v}_{x2}(t+\Delta t) - \mathrm{v}_{x2}(t)\right]/\overline{V}\Delta t \tag{2.18}$$

The frequency is defined by the time interval Δt: f=1/ Δt. With this technique, enstrophy spectra itself can be measured. Enstrophy is defined as.

$$e(f) = \left\langle \left|\omega(f)\right|^2 \right\rangle \tag{2.19}$$

In order to obtain information about the flow fields, Vorobieff et al. [21] developed a digital particle imaging velocimetry (DPIV) system (Fig. 2.6). Originally, the particle imaging velocimetry (PIV) is an optical method used to obtain instantaneous velocity measurements and related properties in fluids. The fluid is seeded with tracer particles which, for the purposes of PIV, are generally assumed to faithfully follow the flow dynamics. It is the motion of these seeding particles that is used to calculate velocity information of the flow being studied. The most important point of PIV is that PIV produces two dimensional vector fields, while the other single-point techniques measure the velocity at a point. With PIV is generally considered cases where the particle concentration is such that it is possible to identify individual particles in an image, but not with certainty to track it between images. Besides, in the soap film case, the PIV images of the soap film flow can be employed to find the local thickness of the film by averaging the intensity of the illuminated light scattered by the seeding particles. As mentioned above, Vorobieff et al. developed the DPIV system which simultaneously records velocity and thickness fields of flowing soap films (Fig. 2.7). With this technique, the experimental and numerical studies which describe the flow field have been developed.

Nowadays, the spatially local scale-to-scale energy and enstrophy transport information are

obtained by the measured velocity and vorticity field [22-24].

2.3.6. Effects of polymer in flowing soap films as a 2D turbulence

As mentioned in chapter 1, the characteristics of turbulence are changed by polymer additives. This phenomena is called drag reduction in 3D turbulence. For this phenomenon, polymers which have long maximum relaxation time τ are effective. The maximum relaxation time of the polymers are defined as

$$\tau \approx \frac{\eta R_g^{\ 3}}{k_B T} \tag{2.20}$$

where η is the solvent viscosity, R_g is the radius of gyration, k_B is the Boltzmann constant and T is the temperature. To have larger maximum relaxation time, long, flexible and linear polymer is effective. Indeed the molecular weight should have at least 10^6 orders. Thus, high molecular weight of polyethylene oxide is used very often for the drag reduction, which is a long-standing issue in 3D turbulence. In more recent, it appears that the effect of polyethylene oxide in 2D turbulence is different from that of 3D.

Amarouchene et al. [10] showed the velocity power spectra of 2D turbulence for different polyethylene oxide concentrations. As shown in Sec. 2.3.4, the energy density spectrum $E(k)$, that is, the velocity power spectra of 2D turbulence is predicted to have two different scaling. For scales larger than the injection scale l_{inj}, $E(k)$ scales as $k^{-5/3}$, while for smaller scales $E(k)$ scales as k^{-3}. Amarouchene et al. showed that the power spectra of the velocity components are reduced by polyethylene oxide as long flexible polymer additives in amplitude of the low frequencies or the large scales, which is the most important result. On the other hand, the high frequency part of the velocity power spectra, which corresponds to the small scales, is hardly affected by addition of the polymer (Fig. 2.8.a). The power component of the scaling shows still -3. Not only the velocity power spectra but also the probability density function (pdfs) of the velocity fluctuations and the third moment of longitudinal velocity differences

$$S_3(r) = \left\langle \delta u^3(r) \right\rangle = \left\langle \left(u(y+r) - u(y) \right)^3 \right\rangle \tag{2.21}$$

are discussed (the brackets indicate temporal averaging or ensemble averaging). The pdfs of the velocity fluctuations became narrower by the polymer additives (Fig. 2.8.a). Besides, the third moment was suppressed by the polymers (Fig. 2.8.b). Indeed, the presence of the polymer affects not only the mean value of $u^3(r)$ as seen through $S_3(r)$ but also affects the fluctuations of this quantity. The pdfs of $u^3(r)/r$ which has the dimensions of an energy transfer rate is also suppressed by the polymer additives (Fig. 2.8.b). The scaling value of the thickness fluctuations also shows the suppression of the inverse energy cascade. By considering all the fact, Amarouchene et al. suggested that the polymer mainly suppress the large scale fluctuation in 2D turbulence.

Boffetta et al. [25] explained the work of Amarouchene et al. by considering the viscoelastic solution model.

$$\partial_t \mathbf{u} + (\mathbf{u} \bullet \nabla)\mathbf{u} = -\nabla p + \nu \Delta \mathbf{u} + \frac{2\eta\nu}{\tau} \nabla \bullet \boldsymbol{\sigma} - \alpha \mathbf{u} + \mathbf{f}, \tag{2.22}$$

$$\partial_t \boldsymbol{\sigma} + (\mathbf{u} \bullet \nabla)\boldsymbol{\sigma} = (\nabla \mathbf{u})^T \bullet \boldsymbol{\sigma} + \boldsymbol{\sigma} \bullet (\nabla \mathbf{u}) - \frac{(\boldsymbol{\sigma} - l)}{\tau}. \tag{2.23}$$

The velocity field $\mathbf{u}$ is incompressible, the symmetric matrix $\boldsymbol{\sigma}$ is the conformation tensor of polymer molecules, and its trace tr$\boldsymbol{\sigma}$ is a measure of their elongation. The parameter τ is the slowest polymer relaxation time. The energy source $\mathbf{f}$ is a large-scale random, zeromean, statistically homogeneous and isotropic, solenoidal vector field. The pressure term $-\nabla p$ is ensures incompressibility of the velocity field. The matrix of velocity gradients is defined as $(\nabla \mathbf{u})_{ij} = \partial_i u_j$ and l is the unit tensor. The solvent viscosity is denoted by ν and η is the zeroshear contribution of polymers to the total solution viscosity $\nu_t = \nu(1+\eta)$. The dissipative term -$\alpha\mathbf{u}$ models the mechanical friction between the soap film and the surrounding air. And then, the average kinetic energy balance in the statistically stationary state can be obtained from Eq. (2.22) and Eq. (2.23),

$$F = \epsilon + \frac{2\eta\nu}{\tau^2}\left(\langle \mathrm{tr}\boldsymbol{\sigma} \rangle - \mathrm{tr} l\right) + \alpha \left\langle |\mathbf{u}|^2 \right\rangle \tag{2.24}$$

where $\epsilon = \nu \left\langle |\nabla \mathbf{u}|^2 \right\rangle$ is the viscous dissipation and F is the average energy input, which is flow-independent for a Gaussian, δ-correlated random forcing $\mathbf{f}$. Since in two dimensions the kinetic energy flows towards large scales, it is mainly drained by friction, and viscous dissipation is vanishingly small in the limit of very large Reynolds numbers. That is why ϵ can be neglected in the

Newtonian case (η=0) balance fields. In the Newtonian case, Eq. (2.24) can be

$$F = \alpha \left\langle |\mathbf{u}|^2 \right\rangle_N \tag{2.25}$$

since the polymer doesn't exsits. Then the following equation can be obtained from Eq. (2.23) and Eq. (2.24)

$$\left\langle |\mathbf{u}|^2 \right\rangle = \left\langle |\mathbf{u}|^2 \right\rangle_N - \frac{2\eta\nu}{\alpha\tau^2}\left(\langle \mathrm{tr}\boldsymbol{\sigma} \rangle - \mathrm{tr}l\right) \tag{2.26}$$

As a consequence of incompressibility and chaoticity of the flow, it can be shown from Eq. (2.23) that $\mathrm{tr}\boldsymbol{\sigma} \geq \mathrm{tr}l$, that is why $\left\langle |\mathbf{u}|^2 \right\rangle \leq \left\langle |\mathbf{u}|^2 \right\rangle_N$. As viscosity dissipation tends to zero in 2D flows, the average polymer elongation increases so as to compensate for the factor ν in Eq. (2.26), resulting in a finite effect also in the infinite *Re* limit. Since energy is essentially dissipated by linear friction, the depletion of $\left\langle |\mathbf{u}|^2 \right\rangle$ entails immediately the reduction of energy dissipation. The main difference between 2D *friction reduction* and 3D drag reduction resides in the length scales involved in the energy drain—large scales in 2D vs small scales in 3D. Besides, the following equation which describes the probability density function of the velocity component u_x is suggested.

$$\mathrm{P}(u_x) = N \exp\left(-c|u_x|^b\right) \tag{2.27}$$

The velocity component will show the intermittency by polymer additives.

Indeed, it was believed that only the friction reduction can be happen in 2D turbulence by polymer additives. However, in the recent research, Kellay [11] showed the reduction of the enstrophy flux fluctuations operates at small scales when the strain present are comparable to the inverse relaxation time of the polymer (the distribution of enstrophy flux divided by a length scale is a measure of the distribution of strain rates). This result shows that the drag reduction can also be discuss in 2D turbulence. Besides, the Eq. (2.27) is confirmed experimentally in Kellay's work [11]. Polymers can affect the small scale and large scale in 2D turbulence.

2.4. Conclusion

The experimental technique to observe the 2D flow has been developed from the middle of 1990s. In the first stage, the single-point measurement using a LDV and the scaling law analysis was only the technique to measure the turbulence and it is still useful. In order to measure the *flow field*, two-pointes measurement and PIV has developed. These observations could detect the scaling law of inverse energy cascade and enstrophy cascade in 2D turbulence. Polymer additives mainly affect the inverse energy cascade in larger scale of 2D flow. However, Kellay et al. suggest that the polymer can also affect on the enstrophy flux fluctuations in recent studies. The probability density of the velocity fluctuation can also detect the effects of polymer. Historically, the single image analysis of the 2D flow is quite rare. However, since the soap film show the flow information on the interference pattern by reflecting the illumination light, thus, the new analytical method to analyze the interference pattern should be developed, which is shown in this thesis.

2.5. Reference

[1] H. Kellay, W. I. Goldburg, Two-dimensional turbulence: a review of some recent experiments, *Rep. Prog. Phys.* **65**, 845 (2002)

[2] M. A. Rutgers, X. L. Wu, W. B, Daniel, Conducting fluid dynamics experiments with vertically falling soap films, *Rev. Sci. Instrum.* **72**, 3025 (2001)

[3] Y. Couder, Two-dimensional grid turbulence in a thin liquid film, *J. Phys. (France). Lett.* **45**, 353 (1984)

[4] Y. Couder, C. Basdevant, Experimental and numerical study of vortex couples in two-dimensional flows, *J. Fluid. Mech.* **173**, 225 (1986)

[5] M. Gharib, P. Derango, A liquid film (soap film) tunnel to study two-dimensional laminar and turbulent shear flows, *Physica. D.* **37**, 406 (1989)

[6] M. Beizaie, M. Gharib, Fundamentals of a liquid (soap) film tunnel, *Exp. Fluids.* **23**, 130 (1997)

[7] R. H. Kraichnan, Inertial ranges in two-dimensional turbulence, *Phys. Fluids.* **10**, 1417 (1967)

[8] G. K. Batchelor, Computation of the energy spectrum in homogeneous two-dimensional

turbulence, *Phys. Fluids. Suppl.* **II**, II-233 (1969)

[9] J. Sommeria, Experimental study of the two-dimensional inverse energy cascade in a square box, *J. Fluid. Mech.* **170**, 139 (1986)

[10] Y. Amarouchene, H. Kellay, Polymers in 2D turbulence: Suppression of large scale fluctuations, *Phys. Rev. Lett.* **89**, 104502 (2002)

[11] H. Kellay, Polymers suppress the inverse transfers of energy and the enstrophy flux fluctuations in two-dimensional turbulence, *Phys. Rev. E.* **70**, 036310 (2004)

[12] H. Kellay, X. L. Wu, W. I. Goldburg, Experiments with turbulent soap films, *Phys. Rev. Lett.* **74**, 3975 (1995)

[13] H. Kellay, X. L. Wu, W. I. Goldburg, Vorticity measurements in turbulent soap films, *Phys. Rev. Lett.* **80**, 277 (1998)

[14] A. Belmonte, W. I. Goldburg, H. Kellay, B. Martin, X. L. Wu, Velocity fluctuations in a turbulent soap film: The third moment in two dimensions, *Phys. Fluids.* **11**, 1196 (1999)

[15] B. K. Martin, X. L. Wu, W. I. Goldburg, M. A. Rutgers, Spectra of decaying turbulence in a soap film, *Phys. Rev. Lett.* **80**, 3964 (1998)

[16] M. A. Rutgers, Forced 2D turbulence: Experimental evidence of simultaneous inverse energy and forward enstrophy cascades, *Phys. Rev. Lett.* **81**, 2244 (1998)

[17] C. H. Bruneau, O. Greffier, H. Kellay, Numerical study of grid turbulence in two dimensions and comparison with experiments on turbulent soap films, *Phys. Rev. E.* **60**, R1162 (1999)

[18] C. H. Bruneau, H. Kellay, Experiments and direct numerical simulations of two-dimensional turbulence, *Phys. Rev. E.* **71**, 046305 (2005)

[19] O. Greffier, Y. Amarouchene, H. Kellay, Thickness Fluctuations in Turbulent Soap Films, *Phys. Rev. Lett.* **88**, 194101 (2002)

[20] H. Kellay, C. H. Bruneau, X. L. Wu, Probability density functions of the enstrophy flux in two dimensional grid turbulence, *Phys. Rev. Lett.* **84**, 1696 (2000)

[21] P. Vorobieff, M. Rivera, R. E. Ecke, Soap film flows: statistics of two-dimensional turbulence, *Phys. Fluids.* **11**, 2167 (1999)

[22] M. K. Rivera, W. B. Daniel, S. Y. Chen, R. E. Ecke, Energy and enstrophy transfer in decaying two-dimensional turbulence, *Phys. Rev. Lett.* **90**, 104502 (2003)

[23] S. Chen, R. E. Ecke, G. L. Eyink, X. Wang, Z. Xiao, Physical mechanism of the

two-dimensional enstrophy cascade, *Phys. Rev. Lett.* **91**, 214501 (2003)

[24] T. Shakeel, P. Vorobieff, Decaying turbulence in soap films: energy and enstrophy evolution, *Exp. Fluids*. **43**, 125 (2007)

[25] G. Boffetta, A. Celani, S. Musacchio, Two-dimensional turbulence of dilute polymer solutions, *Phys. Rev. Lett.* **91**, 034501 (2003)

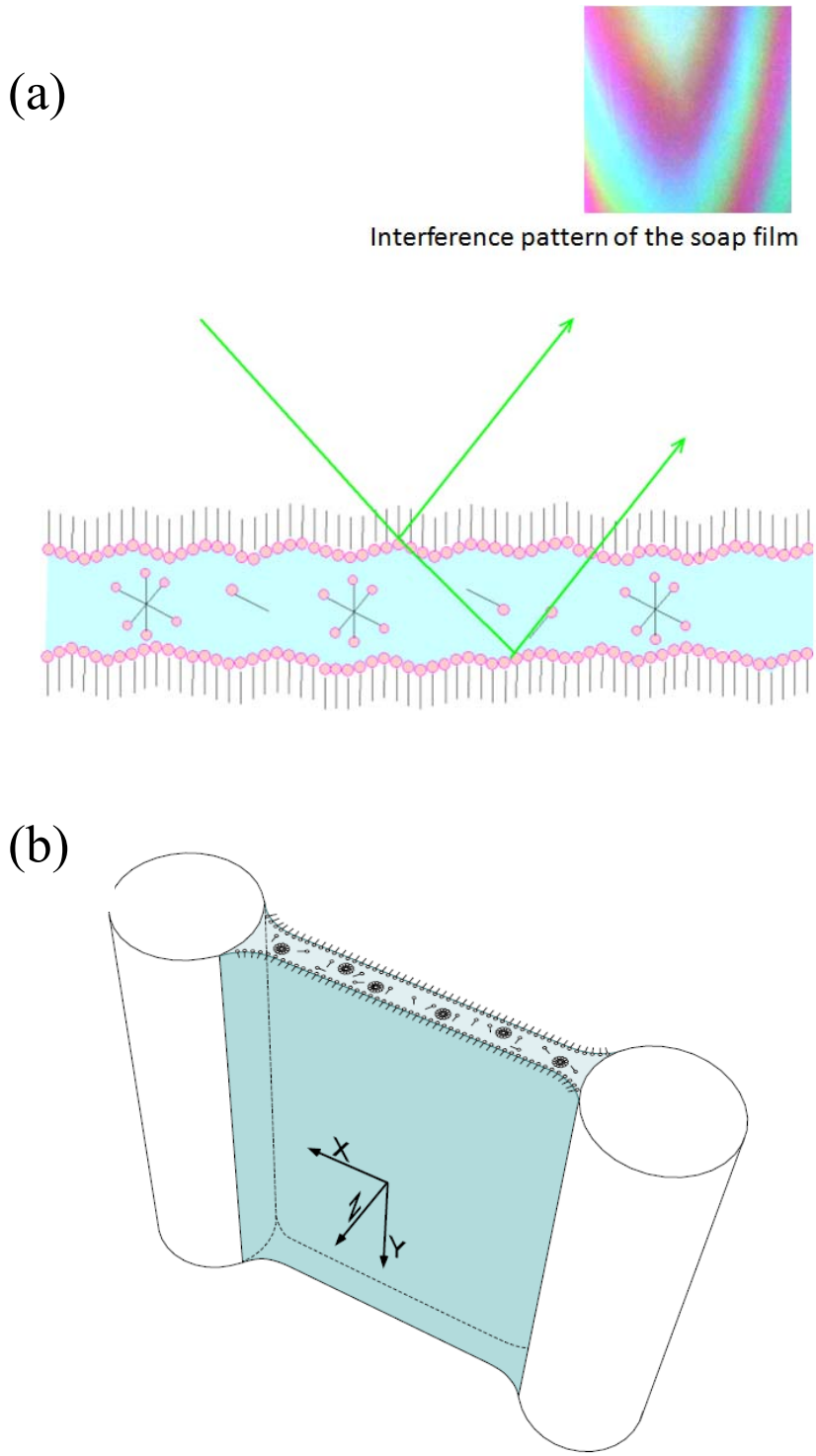

Figure 2.1. (a) Schematics of a soap film cross section. Soap film reflect the illumination light in the front and back of the film, these reflecting light make the interference pattern on the soap film, which is caused by the thickness of the film. (b) Cross sectional diagram of a soap film spanning the gap between two vertical wires [2].

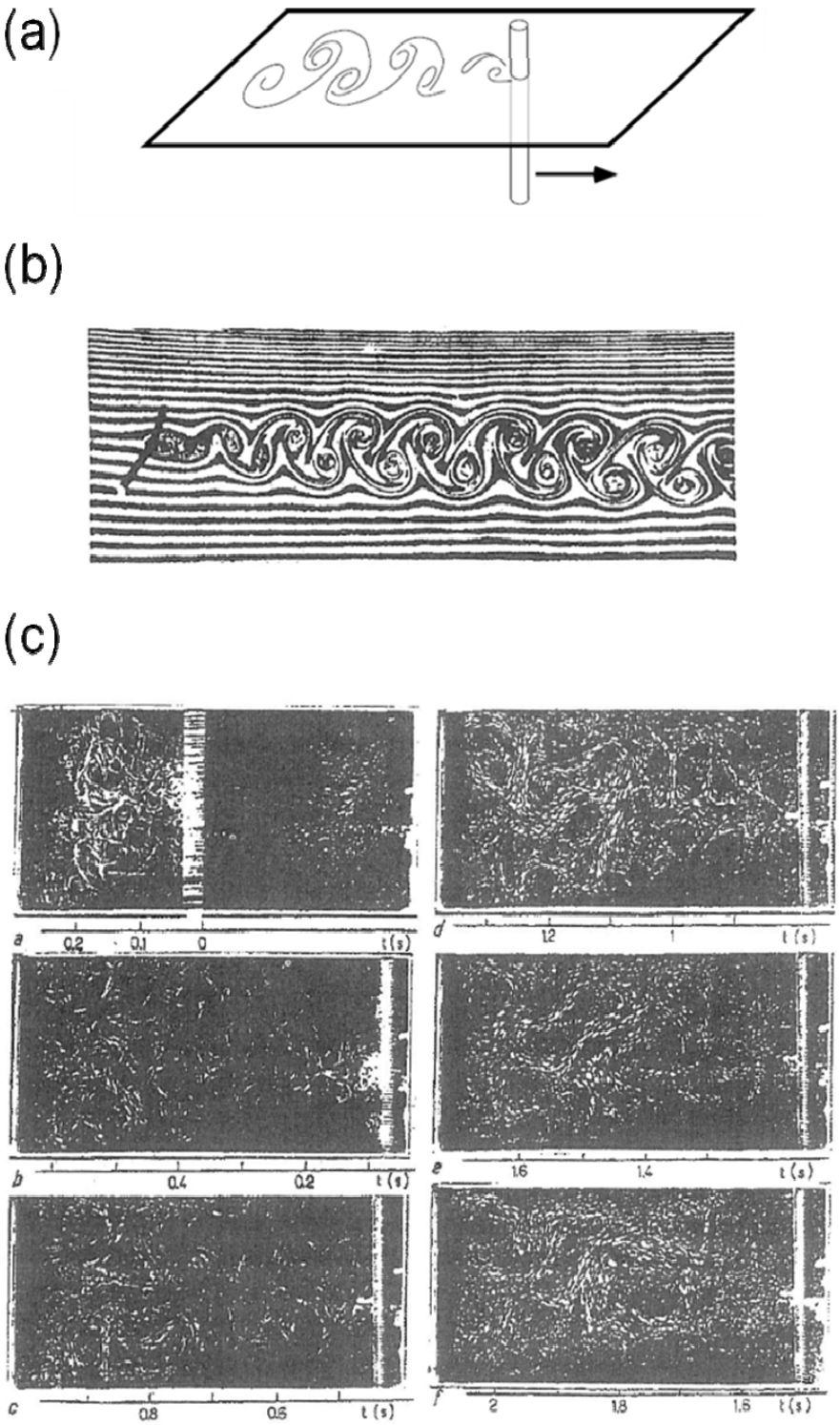

Figure 2.2. (a) First experimental apparatus for 2D fluids made by Couder [2, 3]. (b) Karman vortex taken by Couder [3] (c) 2D turbulence taken by Couder [3], which shows the vortices became lager over time.

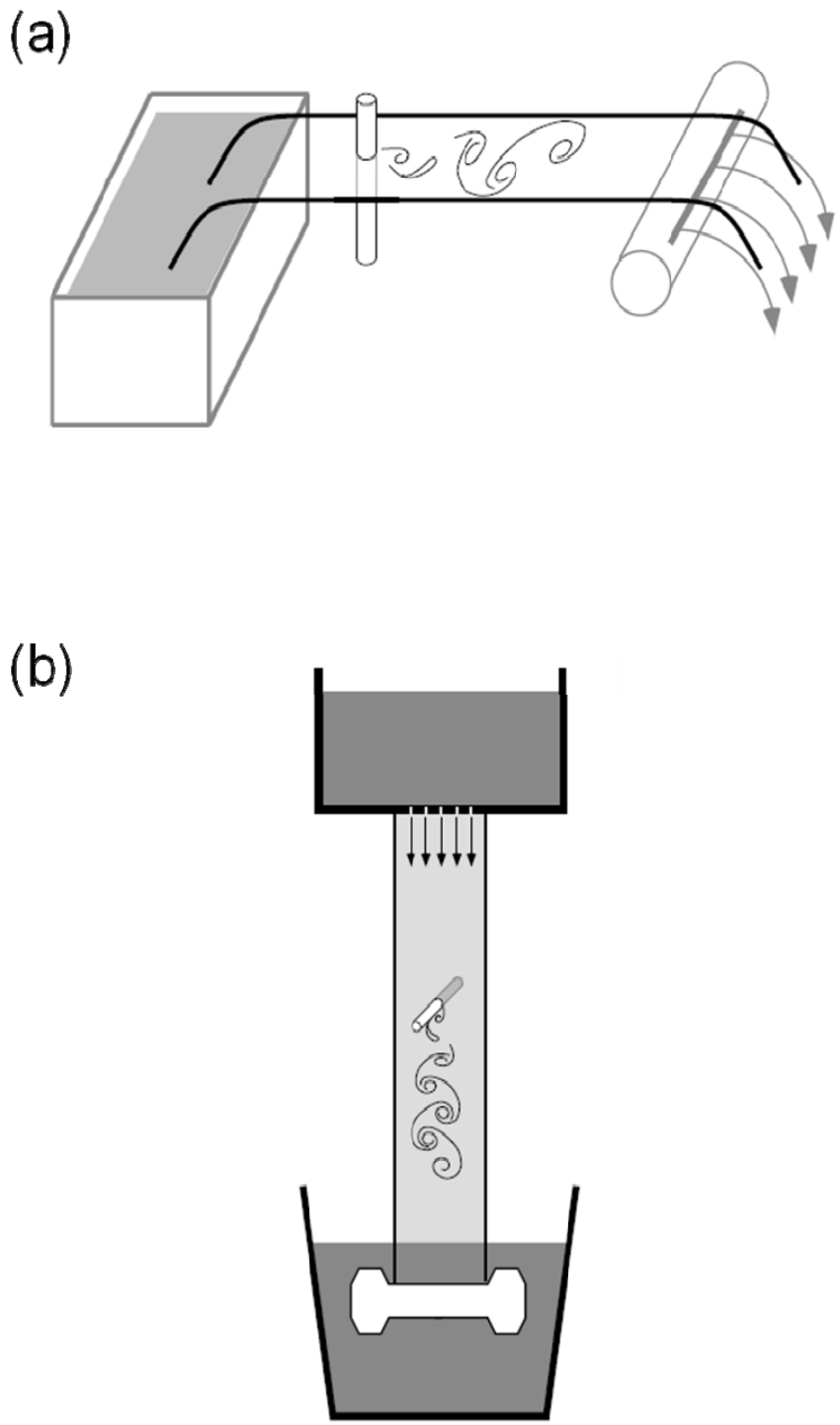

Figure 2.3. (a) The horizontal 'soap tunnel' draws a film from a reservoir, across rigid rails, onto a moving water sheet [2, 5]. (b) An earlier version of the vertically falling soap film [2, 12].

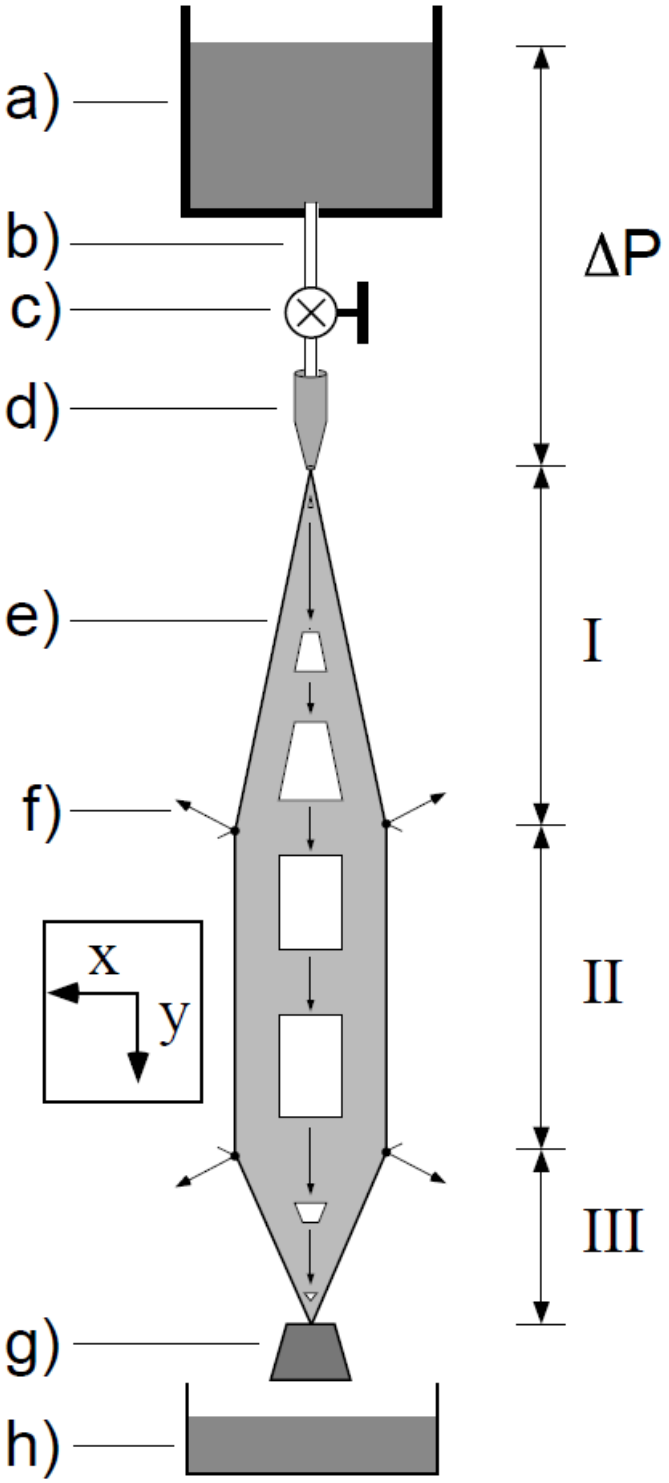

Figure 2.4. Diagram of a vertically flowing film showing the evolution of a constant volume of soap solution. Precise explanation is in Sec 2.3.2. [2].

$$\omega = \frac{1}{2}\left[\mathrm{v}_{y2}(t) - \mathrm{v}_{y1}(t) + \mathrm{v}_{y2}(t+\Delta t) - \mathrm{v}_{y1}(t+\Delta t)\right]/\Delta x$$
$$-\frac{1}{2}\left[\mathrm{v}_{x1}(t+\Delta t) - \mathrm{v}_{x1}(t) + \mathrm{v}_{x2}(t+\Delta t) - \mathrm{v}_{x2}(t)\right]/\overline{V}\Delta t$$

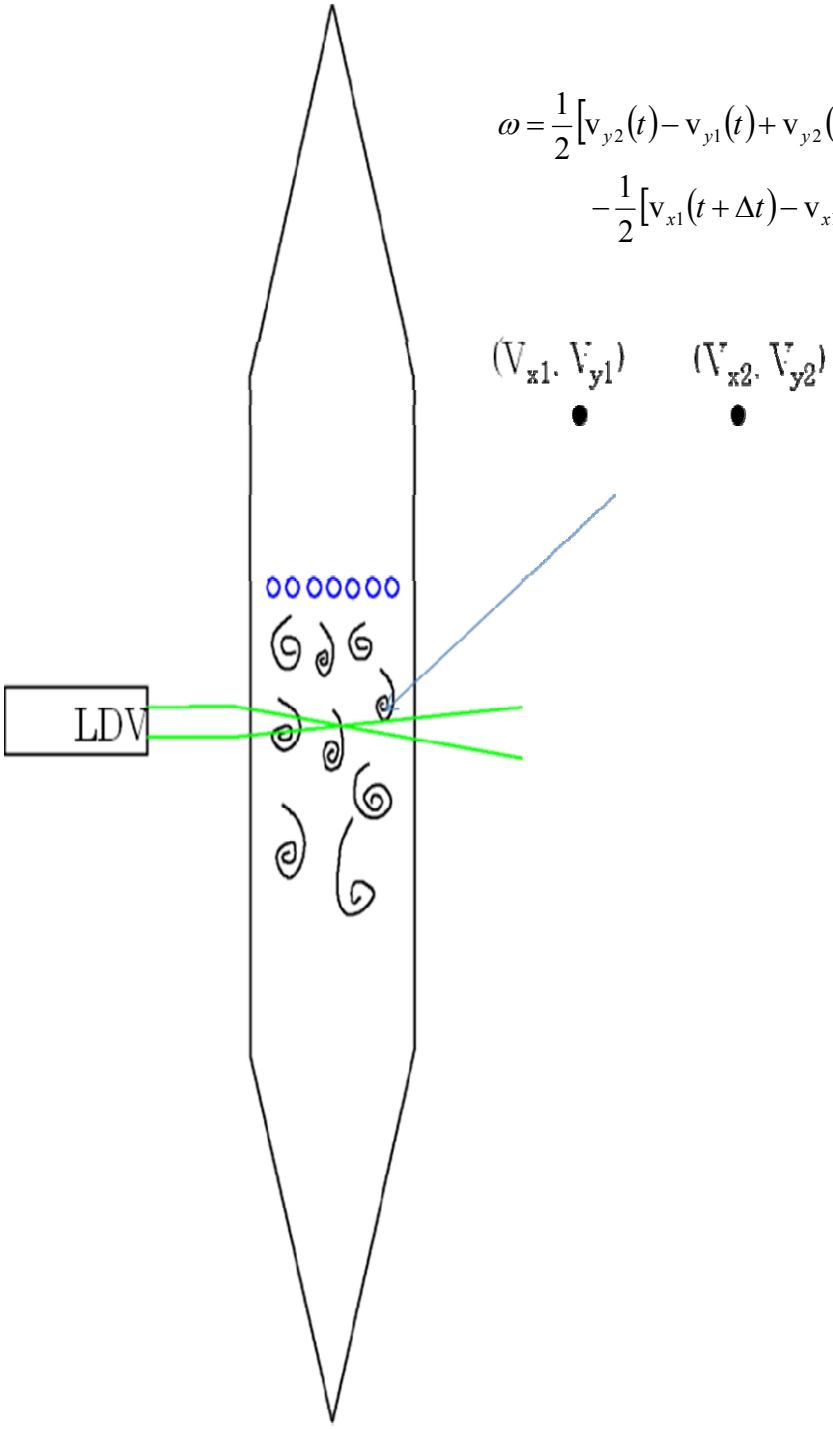

Figure 2.5. Schematic of two-points measurement for the observation of the vorticity.

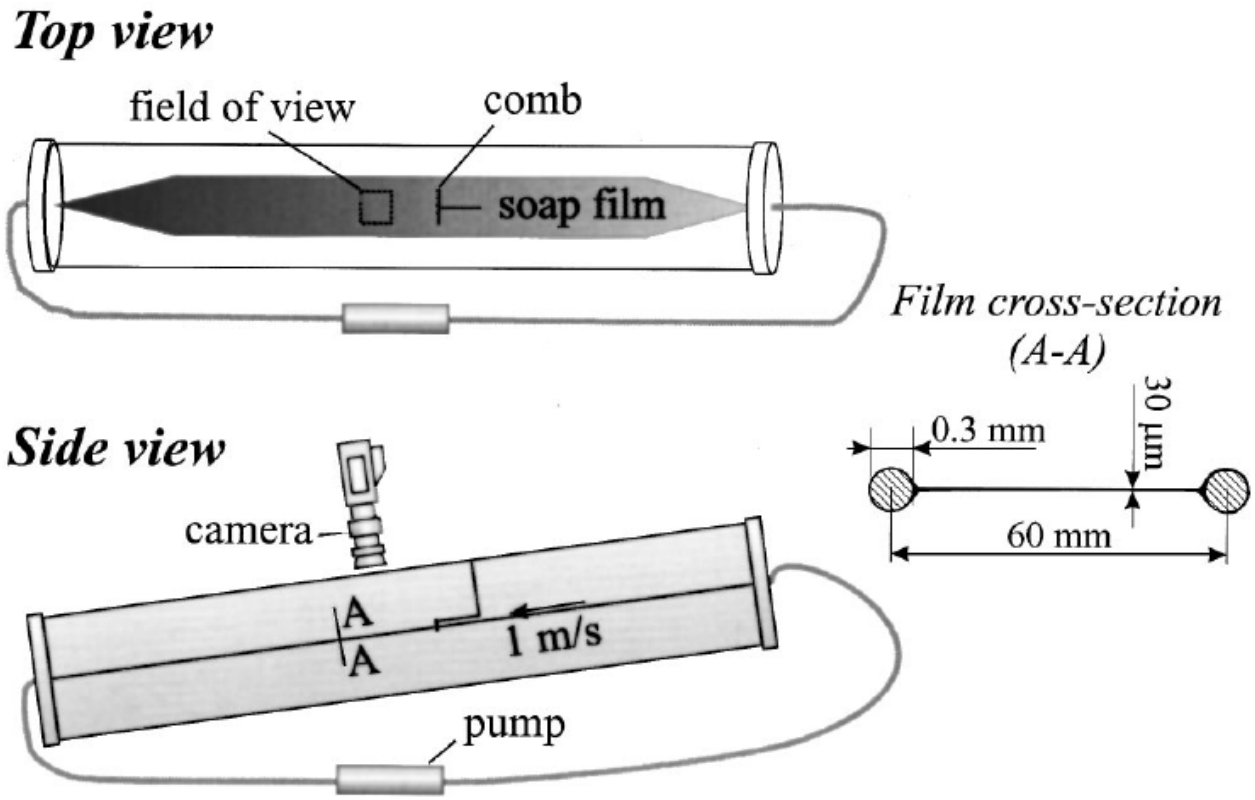

Figure 2.6. Schematic diagram of PDIV experimental setup [21].

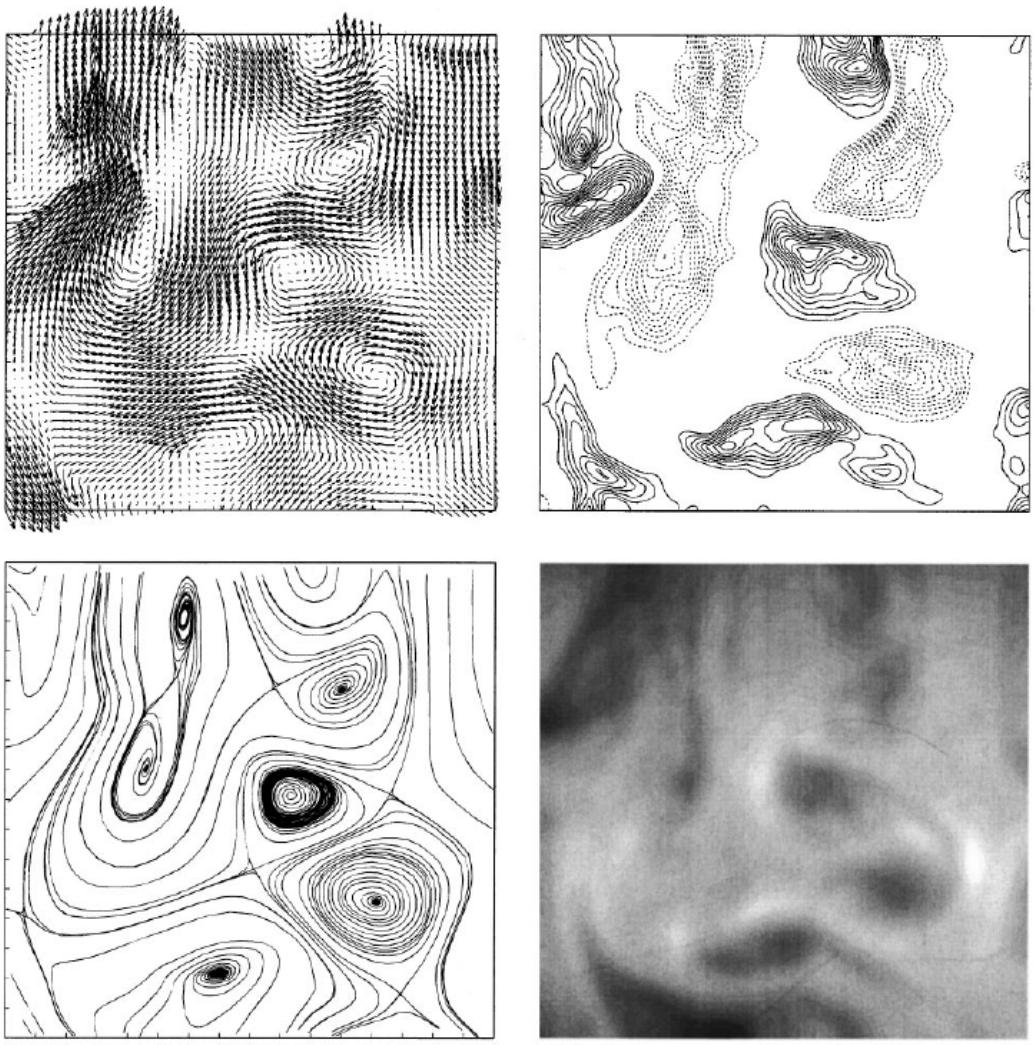

Figure 2.7. An example of the instantaneous flow pattern 1 cm downstream from the comb: velocity field (top left), vorticity contours (top right), instantaneous streamlines (bottom left), thickness (bottom right) [21].

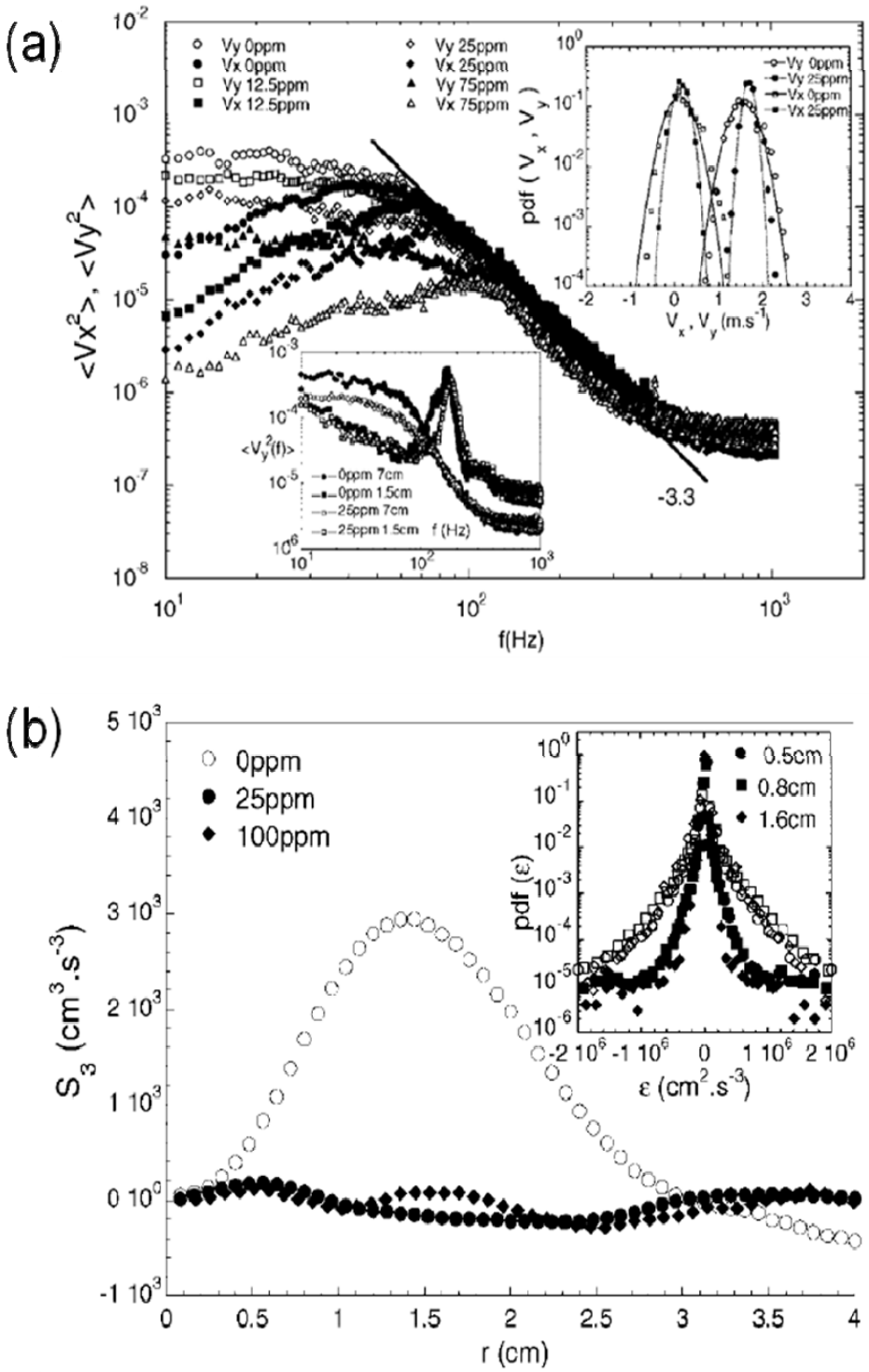

Figure 2.8. (a) Longitudinal (V_x) and transverse (V_y) velocity power spectra for time frequency f(Hz) for different polyethylene oxide concentrations as indicated in ppm (4×10^6 molecular weight) at a distance of 7 cm from the grid and a flux of 0.4 ml/s. inset; Upper inset: pdfs of V_x and V_y for similar conditions. (b)$S_3(r)$ for different polyethylene oxide concentrations at the same position to (a). [10].

Chapter 3

Image Analysis of Thickness in Flowing Soap Films and Effects of Polyethylene Oxide on the Flow

3.1. Abstract

Two-dimensional turbulence in flowing soap films with polymer additives is analyzed by the interference image analysis, that is, IFI method. The power spectra of the interference patterns of turbulent soap films were calculated. The scaling exponent of the power spectrum was -5/3 for polymer free solution and -1 for dilute polymer solution in enstrophy cascade range, which is consistent with the results of thickness fluctuations in previous researches. A Curvature analysis method is proposed, which calculates the curvatures of the interference pattern of turbulent soap films. The results suggest that the curvature histogram describes well the shape of the interference pattern, which is related to the shape of the vortices. The curvature histograms for different polymer concentrations can be fitted by a distribution function which is proposed to quantify probability density function of the velocity fluctuations in a previous research. The velocity fluctuations are also discussed by the color distributions.

3.2. Introduction

Two-dimensional turbulence has been a fascinating topic since Kraichnan and Batchelor's original work [1, 2]. They made predictions of the behavior of statistical quantities describing the flow. The scaling law is the main technique which characterizes the flow. Not only meteorologists and oceanographers but also theorists who solve the Navier-Stokes equations numerically have paid attention to the two-dimensional (2D) turbulence, since 2D flow is much less complex than three-dimensional (3D) turbulence to solve equations computationally. Couder and coworkers [3, 4], Gharib and Derango [5] undertook the pioneering work of 2D turbulence in laboratories. Flowing soap films are one example of quasi-2D turbulence. In 2D turbulence, an inverse energy cascade occurs from the injection scale to the larger scale, which is the most different feature from 3D turbulence. From the injection scale to the smaller scale, an enstrophy cascade occurs. Many experiments have been made in order to confirm the scaling law for each physical value in these cascade ranges [6-16].

Thickness fluctuations of 2D turbulence were investigated by Greffier et al. [15]. Besides,

Amarouchene et al. [16] reported the effects of polymers on 2D turbulence properties by considering the scaling law of thickness fluctuations. The power spectrum of the thickness fluctuations in the turbulent soap films shows a scaling law,

$$\left\langle h^2(f)\right\rangle \equiv \left\langle h^2(k)\right\rangle \sim f^{\alpha} \sim k^{\alpha} \tag{3.1}$$

where f is a frequency in time scale, which can be converted to a length scale l if we consider the Taylor frozen turbulence hypothesis $k=2\pi/l=2\pi f/V$, where k is the longitudinal wave number in the direction of the mean velocity V [16]. In the polymer free solution case, the power component α in Eq. 3.1 is -5/3 in the enstrophy cascade range. The power component α becomes close to -1 in the presence of polymer. The polymer suppresses the inverse transfers of energy, and then only enstrophy dominates the thickness fluctuations. This is the reason why the power component α approaches -1 with polymer additives.

The velocity fluctuations in a 2D turbulent soap film were presented by Belmonte et al. [10], Amarouchene et al. [16] and Kellay [9]. The probability density function of the velocity fluctuations becomes narrower with polymer additives. Kellay [9] confirmed that the probability density function can be fitted by a sub-Gaussian and a super-Gaussian function: $N\exp(-c|u|^{\gamma})$[9, 17].

These experimental studies usually employed single-point measurements of the flow via laser Doppler velocimetry (LDV). The single-point measurement was the only major technique used for soap films analysis that was why to have precise thickness field was difficult. Kellay et al. [7] reported vorticity fluctuations by using two points measurements on decaying flowing soap films. In order to obtain information about the flow fields, Rivera et al. and Vorobieff et al. [18, 19] developed a digital particle imaging velocimetry (DPIV) system which simultaneously records the velocity and thickness fields of flowing soap films. The flow field can be observed intuitively with the DPIV method. With these techniques, the experimental and numerical studies which describe the flow field have been developed. Nowadays, the spatially local scale-to-scale energy and enstrophy transport information are obtained by the measured velocity and vorticity field [20-22].

Very few researches based on single-image measurements were reported [23, 24]. In this chapter, the original ways of image analysis are proposed for 2D turbulent soap films study [25]. The soap films exhibit colors variations caused by thickness fluctuations, due to optical interferences between the front and back surfaces of the film. Therefore, the interference patterns show the information of the thickness. Thus, the original analysis is named IFI method which

analyzes the turbulence with only one interference image (IFI). The interference patterns were recorded by a video camera and quantified by the IFI method. Besides, polyethylene oxide (PEO) as a polymer was added on the flow in order to change the turbulence, which is also quantified by the IFI method. IFI method includes three types of analyses, that is, Fourier transformation method, Curvature analysis method and Color distribution analysis method.

3.3. Experimental

3.3.1. Experimental arrangement

The measurements were performed by using a design of the soap film channel which closely follows the description of Rutgers et al. [26]. A schematic of the setup is shown in Fig. 3.1. The experimental apparatus consists of the upper supply reservoir (a) and the bottom collection reservoir (e). Two 1 mm diameter nylon wires splay from the nozzle (c). The wires are stretched from top to bottom with the tensioning weight (d). Thinner threads pull the guide wires and hold them apart. The channel is 10 cm wide and 90 cm long. The soap solution is flowing between two parallel wires from the upper reservoir to the bottom reservoir under the action of gravity. The mean speed of the flow can be adjusted by the valve (b). The channel has three sections: the expansion section (f), the test section (g) and the contraction section (h). In the beginning of the test section, a grid of equally spaced 8 cylinders (i) is inserted. The diameter of the cylinders is 0.3 cm and the spacing between the cylinders is 0.6 cm. Turbulence was produced under the grid. The eddies in turbulence are convected by the mean flow without much deformation. Therefore, the mean velocity was calculated from the convected distance of the eddies, which was taken by the video camera in 1/60 seconds. The calculated mean velocity is approximately 130 cm/s.

The film was illuminated by a commercial white light source (EFA25EN/22, TOSHIBA Co.). According to the data sheet provided by the manufacturer, the wavelengths of this illumination range from 400 to 720 nm. More precisely, the excitation spectrum is composed of a major narrow peak at 540 nm and several minor narrow peaks at 400, 430, 460, 480, 540, 600, and 710 nm (Fig. 3.2). Generally, monochromatic light source like a sodium lamp (589 nm) is used for soap film experiments in order to avoid the interference of the reflected light in many wave numbers. A

commercial white light source was selected here, however, the 540 nm wave length (the light colors green) was the strongest one in this light sores, beside only the green channel of the image was used for the analysis, thus the illuminated light can be treated as if it is monochromatic light source. Beside, the 589 nm generated by sodium lamp is difficult to detect with the commercial video camera. Thus, to use the commercial white light source (EFA25EN/22, TOSHIBA Co.) to illuminate the soap film is reasonable.

The polymer used was polyethylene oxide (PEO), which was obtained from Wako Pure Chemical Industries. The molecular weight was 4×10^6, average degree of polymerization n is about 90900. PEO was diluted in the soap solution ranging from 5 parts per million by weight (ppm) to 30ppm. The soap solution contained 1.8 % of surfactant from a commercial detergent. The commercial detergent includes stabilization agents, however the stabilizer has not enough molecular weight to inhibit the turbulence, that is, these stabilizers will not be problem for the experiments. That is why, to use commercial detergent is reasonable to make the soap film easily.

3.3.2. Data acquisition

The interference images of soap films were recorded with a digital video camera (Panasonic NV-GS250) at the data acquisition area which was 20 cm behind the grid. The shutter speed of the video camera is 1/3000 second. A time interval in a series of images can be adjusted to 1/60 second by using the software FEATHER made by CANOPUS Co. Each of the frames acquired by the camera was converted into RGB form files through the capture board (CANOPUS: MTV2000P) at a light intensity resolution of 24-bit color and a spatial resolution of 640×480 pixels. A part of the image which corresponds to the data acquisition area (j) in Fig. 3.1 was clipped. The size of the image is 256×256 pixels, which corresponds to 2.46×2.46 cm^2. Five images were acquired for each soap solution as experimental data.

3.4. Background ideas for the analysis and method of data analysis

A major change in this work compared to the previous works is the method of data analysis. In this research, only one interference image is used in order to analyze the characteristics of 2D decaying turbulence, which is named IFI method. IFI method includes three kinds of image analysis methods. First one is a 2D Fourier transformation analysis, the second one is a Curvature analysis and the third one is a Color distribution analysis. Each software analyzes the interference pattern of soap films based on the intensity of the green channel, which has the biggest contrast compared to red color and blue color data. With this technique, the analysis of turbulence become much simple, and it is possible to discuss large area of the instantaneous turbulent flow, while the previous work like a LDV can only make 1 point observation.

Softwares for image analysis and curve fitting were coded by Delphi (Borland Software Co.). The fitting function is estimated for all data curves by using the nonlinear-least squares method based on the quasi-Marquardt algorithm as a software part of PLASMA [27-33].

3.4.1. The order of the interference in the soap film image.

The intensity of the green channel was analyzed, which was based on the idea that the green color intensity was related to the thickness of the soap film. Why the green channel is related to the thickness? In order to explain this question, it is needed to certify that the order of the interference is not changed in the image, or else the color intensity can be cycled depending on the interference order due to the thickness.

The mean thickness can be estimated from the relation $h=Q/VW$, where Q is the flow flux, V is the mean velocity, W is the channel width. In this experiment, Q was about 0.5 ml/s, V was about 130 cm/s and W was 10 cm. Thus, h was estimated at 3.85 μm. In previous researches, it has already been shown that the thickness fluctuations in vertically flowing films in a turbulent state are typically only 5 % [8]. Thus, the thickness fluctuations were about 190 nm in this experiment. The optical path difference which made the interference pattern was calculated as $2nhcosI'$ shown as Fig. 3.3. n is the refractive index, h is the thickness of the film since the illumination lights are refected

on the front and back of the film, and *I'* is the refraction angle at the back side of the film. In this experiment, *n* was 1.33 as water, *h* was 190nm, *cosI'* was assumed as 1. Thus, 2*nhcos I'* was about 500 nm. By considering the data sheet of the illumination provided by the manufacturer (Fig. 3.2), the color distribution of the soap film image which is shown in Fig. 3.1 and Fig. 3.8, and only the green channel was used for the calculation, the reflected light can be assumed as 540 - 600 nm, mainly around 540nm. The optical path difference which was calculated as 500 nm was less than one wave length as 540 nm, thus, it was thus reasonable to consider that the interference order couldn't be changed in the local image analysis in this experiments. That was why, the intensity of the green channel was related to the thickness.

3. 4.2. IFI method-1: Fourier transformation analysis

The main method to investigate the thickness fluctuations of 2D turbulence was to observe the power spectrum of the thickness varying with time which is calculated by the velocity varying with time which is obtained by using LDV (See Introduction). In this paragraph, the main method is precisely described and the single-image image analysis, that is, IFI method is proposed.

The mean thickness can be estimated from the relation $h=Q/VW$. The mean velocity V is observed by LDV. The power spectrum of the mean thickness is calculated by

$$\left\langle h^2(f)\right\rangle = \int_{-\infty}^{+\infty} \left\langle h(0)h(t)\right\rangle e^{ift} dt \tag{3.2}$$

where f is a frequency in time scale. Eq. 3.2 can be converted to a length scale l if we consider the Taylor frozen turbulence assumption, which assumes that the small-scale eddies are swept by the mean flow past the observation point without suffering much change. That is, this assumption suggests

$$f = \frac{kV}{2\pi}, \qquad t = \frac{l}{V} \tag{3.3}$$

, where k is the longitudinal wave number in the direction of the mean velocity V [16]. Thus, the Eq. 3.2 is converted to

$$\left\langle h^2(k)\right\rangle = \int_{-\infty}^{+\infty}\left\langle h(0)h\left(\frac{l}{V}\right)\right\rangle e^{i\left(\frac{kV}{2\pi}\right)\left(\frac{l}{V}\right)} d\left(\frac{l}{V}\right) \tag{3.4}$$

The power spectrum of the thickness fluctuations in the turbulent soap films shows a scaling law as shown in Eq. 3.1.

In this work, the original way of image analysis, that is, IFI method is proposed, which calculates the power spectrum of the color intensity of the green channel I_G on a length scale k.

$$\left\langle I_G{}^2(k)\right\rangle = \int_{-\infty}^{+\infty}\left\langle I_G(0)I_G(x)\right\rangle e^{ikx}dx \tag{3.5}$$

, where x shows the pixels on the image. Since the color intensity of green channel is related to the thickness, Eq. 3.4 and Eq. 3.5 are comparable (Fig. 3.4). Thus, the Eq. 3.5 can have the same scaling low of Eq. 3.1. This idea is confirmed in this chapter.

The 2D Fourier transformation software as the IFI method-1 calculates the power spectrum $S(k_x, k_y) = \langle I_G{}^2(k)\rangle$ of the green channel with a Hamming window. The k_x and k_y are, respectively, the wave numbers which are perpendicular and parallel to the flow direction in the image, that is,

$$k_x = 1/x, \qquad k_y = 1/y \tag{3.6}$$

, where x and y show the pixels on the image. The soap films thickness is thin enough to observe optical interference effects, even with a polychromatic source (See 3.4.1.). The power spectrum $S(k_x, k_y)$ of the green channel can characterize the strength of the thickness fluctuation on length scales $1/k_x$ and $1/k_y$.

3.4.3. IFI method-2: Curvature analysis

The Curvature analysis software is proposed as the IFI method-2, which calculates the curvatures of the interference pattern of the turbulence. The interference patterns have the information of the thickness fluctuation of the soap film. In previous researches, Rivera et al. [18] and Vorobieff et al. [19] showed that the thickness is related to the vorticity of the flow. Indeed, the vorticity contours fit with the thickness field. Furthermore, since the thickness field is related to the vorticity, it is also related to the instantaneous streamlines. The streamlines are a family of curves that are instantaneously tangent to the velocity vector of the flow. In the 2D turbulence, the

instantaneous velocity filed is changed locally, which is detected as a velocity fluctuation [9, 18, 19]. In this aspect, analyzing the characteristic interference pattern due to the thickness field should give us information of the 2D turbulence, such as, the vortex or the streamlines, etc. Thus, the interference patterns are quantified numerically for each image by calculating the curvatures of the pattern.

The image is analyzed by using a three-step procedure of the Curvature analysis software. The first step involves a Weighted Median Filtering operation of the green channel. The Median Filtering operation is widely used to remove the noise in the image by replacing the value of light intensity in 3-by-3 neighborhood. In the second step, the first step smoothed picture Fig. 3.5(a) is used. A black and white image of turbulence is obtained after a clipping procedure as shown in Fig. 3.5(b). The clipping intensity is decided to get a characteristic interference pattern of the turbulence. In the third step, the contour of the interference pattern is traced (Fig. 3.5(c)), and the curvature κ of the contour is calculated. The curvature of a line on a plane can be calculated by the following equation.

$$\kappa = \frac{|\theta_2 - \theta_1|}{ds} \tag{3.7}$$

where θ_1 and θ_2 are the angles between the axis and the tangent of the line at two contacts (x_1, y_1) and (x_2, y_2), ds is the distance between the two contacts, as shown in Fig.3.5(d). These contacts are selected every 25 pixels along the contour. The value of ds is calculated by two coordinates (x_1, y_1) and (x_2, y_2). The values of curvature are calculated for all of the contours on the image.

Mathematically, the curvature is defined as a variation of direction of the tangent vector on 2 contacts. That is why, if the interference pattern is related to the streamline, it is possible to detect the value which is related to the velocity fluctuation, since the streamline is directly related to the velocity (Fig 3.6).

Five images are treated for the Curvature analysis, the average of the Curvature is described as a histogram. The histogram is normalized by the histogram area. Besides, the histogram is treated by 5-point central moving average for smoothing. The histogram is fitted by a distribution function which is proposed to quantify probability density function of the velocity fluctuations in a previous research [17].

3.4.4. IFI method-3: Color distribution analysis

As mentioned above, the thickness is in inverse proportion to the velocity, that is,

$$h = Q/VW = A_1 \frac{1}{V} \tag{3.8}$$

Besides, the thickness is related to the color intensity I. The relationship is simplified as,

$$h \cong A_2 I + C \tag{3.9}$$

Fig. 3.7 shows the relationship between thickness and color intensity distribution, which is described in Eq. 3.9. Fig. 3.7(a) shows the distribution of the thickness. Here, if a fraction of the thickness fluctuation is written as σ_h, the maximum thickness and minimum thickness are shown as following equations.

$$\begin{aligned} h_{\max} &= \langle h \rangle + \sigma_h \langle h \rangle \\ h_{\min} &= \langle h \rangle - \sigma_h \langle h \rangle \end{aligned} \tag{3.10}$$

, where $\langle h \rangle$ shows the mean thickness. Since the thickness is related to the color intensity I, $\langle h \rangle$, $h_{\max}$ and $h_{\min}$ can be assumed as following equation.

$$\langle h \rangle \cong A_2 I_{\text{peak}} + C \tag{3.11}$$

$$\begin{aligned} h_{\max} &= \langle h \rangle + \sigma_u \langle h \rangle \cong A_2 I_{\max} + C \\ h_{\min} &= \langle h \rangle - \sigma_l \langle h \rangle \cong A_2 I_{\min} + C \end{aligned} \tag{3.12}$$

, where I_{peak}, $I_{\max}$ and $I_{\min}$ are the intensity which shows the peak, maximum and minimum value of the color intensity. As shown in Fig. 3.7 (b), the distribution of color intensity is not always symmetric. Thus, the fraction of color intensity distribution is written as σ_u in the upper half of the color distribution, and as σ_l in the lower half. Combining two equations of Eq. 3.12, A_2 can be derived as

$$A_2 = \frac{2\sigma}{I_{\max} - I_{\min}} \langle h \rangle \tag{3.13}$$

Here, it is assumed that the fraction of color intensity σ can be written by

$$\sigma = \frac{\sigma_u + \sigma_l}{2} \tag{3.14}$$

Combining Eq. 3.9, Eq. 3.11 and Eq. 3.13, the thickness h can be derived as

$$h = \frac{2\sigma}{I_{\max} - I_{\min}} I + \left(\langle h \rangle - 2\sigma \frac{I_{\text{peak}}}{I_{\max} - I_{\min}} \right) \tag{3.15}$$

Since the thickness is in inverse proportion to the velocity, the inverse value of the Eq. 3.15, that is, $1/h$ can be proportion to the velocity. Thus, $1/h - 1/\langle h \rangle$ can be related to the velocity fluctuations. In this work, σ is assumed as a 0.05, since the thickness fluctuations in vertically flowing films in a turbulent state are typically only 5 % [8]. The histogram of $1/h - 1/\langle h \rangle$, that is, $P(1/h - 1/\langle h \rangle)$ is calculated by Color distribution analysis software as the IFI method-3. For the calculation, $\langle h \rangle$ is assumed as 1. Here, the fluctuation is important, the absolute value is not meaning full, that is why, if $\langle h \rangle$ is assumed as 1. The histogram of $P(1/h - 1/\langle h \rangle)$, that is, $P(1/h - 1)$ is fitted by a distribution function. Indeed the function is proposed to quantify probability density function of the velocity fluctuations in a previous research [17].

3.5. Results and Discussion

As shown in Fig. 3.8, the apparent sizes of the eddies became smaller with PEO additives. The patterns of turbulence became long and thin due to the polyethylene oxide effect. The polymer must inhibit vortex mergers, a signature of inverse transfers of energy [16]. These effects of polymer are quantified by the IFI method.

3.5.1. Power spectrum of turbulence images

The power spectra $\langle I_G^2(k) \rangle$ of the interference pattern of the soap film image for polymer free solution, 15 ppm and 30 ppm PEO solution are shown in Fig.3.9. Black color corresponds to the intensity of $\langle I_G^2(k) \rangle$. The power spectrum along the arrow direction (see Fig. 3.9), which is consistent with the wave number k_x, is shown in Fig.3.10. The power spectrum in wave number k_x is related to the thickness fluctuation on length scale $1/k_x$. In other words, the power spectrum in k_x shows the information of the interference patterns of soap films which become thin and long in the mean flow direction with PEO additives. That is why, the power spectra stretch to higher wave

number k_x with polymer additives (Fig. 3.9). The power spectra showed a scaling form $<I_G^2(k_x)> \sim k_x^{\alpha}$, and the scaling range was almost between 0.35 cm and 0.05 cm. In the polymer free case (Fig. 3.9(a)), the power component α was -1.66, which perfectly fitted with the -5/3 predicted value. When the polymers were used, the power component -5/3 ceased to exist. The power component α decreased until -1.37 at 15ppm and came out to be close to -1 at 30ppm (Fig. 3.10(b), (c)). The power law behavior of the spatial power spectrum of the turbulent image in k_x was exactly consistent with the power spectrum of the thickness fluctuations in longitudinal wave number in time scale (see Eq.3.1 and Introduction) [15,16]. The comparison for all the polymer concentration is shown in Fig. 3.11. Amarouchene et al. [16] suggested that the polymer inhibits the inverse transfers of energy, and then only enstrophy dominates the thickness fluctuation in the enstrophy cascade range of the flow. Indeed, the power components of IFI method results totally confirm these conclusions. Therefore, it was suggested that the assumption was totally confirmed (see 3.4.2), and the spatial Fourier transformation method of the image was very reasonable in order to measure the thickness fluctuations affected by the polymer, which inhibits the inverse transfers of energy to larger scale.

3.5.2. Curvature histogram of interference patterns

The curvature of the interference pattern of the turbulence images was calculated by the Curvature analysis software. Fig. 3.12 shows the curvature histogram for different polymer concentrations. As shown in Fig. 3.12, the polymer changes the shape of the histogram. The percentage of the small curvatures increased with the polymer concentration. The curvature is defined by Eq. 3.7, whose meaning is the variation of the tangential direction on the line. When the curvature becomes smaller, the line is becoming straighter. This confirms our qualitative observations since the interference patterns become long and thin when polymers are used. Fig. 3.13 shows the histogram for polymer free solution, 15 ppm and 30 ppm PEO solution. The histogram can be fitted by the following equation:

$$\mathrm{P}(\kappa) = A_1 \exp\left\{-A_2(\kappa)^{\gamma}\right\} \tag{3.16}$$

,where A_1 is a prefactor, A_2 is a positive constant, γ is a power component, κ is the curvature. The solid lines in Fig. 3.13 are the best fit curve for each histogram. All the fitting parameters are listed in Table. 3.1 .

Indeed, Eq. (3.16) is proposed by Boffetta et al. [17] in order to quantify the probability density function of the velocity fluctuations in 2D turbulence, that is,

$$\mathrm{P}(u) = N \exp\left(-c|u|^{\gamma}\right) \tag{3.17}$$

where c is a positive constant, γ is a power component, u is the velocity component. Besides, they evaluated the velocity fluctuations of Newtonian and viscoelastic solutions numerically. As viscoelastic solutions, they considered a dilute polymer solution. Eq. 3.17 was experimentally confirmed by Kellay [9]. Kellay showed that the fitting parameter γ are 3 and 1.8 in polymer free solution and 25 ppm polymer solution, respectively. In IFI method-2, the shape of interference pattern was quantified by a curvature. As mentioned above, the curvature can be related to the velocity fluctuation, since the interference pattern is related to the streamline in 2D turbulence (see 3.4.3.). That is why Eq. (3.17) which is proposed to describe the velocity fluctuations can be fitted to the curvature histogram. In this work, a power component γ was changed from about 1.8 to 0.14. Such a decrease is similar to Kellay's conclusions as shown in Fig. 3.13, which indicate that there is a possibility to discuss the velocity fluctuation by using a Curvature analysis as the IFI method-2.

3.5.3. The velocity fluctuations calculated by Color distribution analysis

The original approach to the velocity fluctuation was made by the Color distribution analysis as the IFI method-3. The color intensity of green channel was analyzed in order to take the value which could be related to the velocity fluctuations. The value, that is, $P(1/h-1)$ is shown in Fig. 3.15, which is fitted by the following equation.

$$\mathrm{P}(1/h-1) = A_1 \exp\left\{-A_2|1/h-1|^{\gamma}\right\} \tag{3.18}$$

The solid lines in Fig. 3.15 are the best fit curve for each histogram. All the fitting parameters are listed in Table. 3.2. Eq. 3.18 is same to Eq. 3.17, which indicate that the value $P(1/h-1)$ also follow the equation which described the velocity fluctuations. Besides, the value of γ is slightly decreased

with the increase of PEO concentration as shown in Fig. 3.16. Eq. 3.18 fits well to $P(1/h-1)$ for polymer free case, while the fitting curve deviate from $P(1/h-1)$ in the edge for 30 ppm case. The value of $P(1/h-1)$ is changed especially in the middle of the distribution $P(0)$ by polymer additives. $P(1/h-1)$ is related to the velocity fluctuation, thus the $P(0)$ is related to the mean velocity. A comparison of the value γ obtained by Eq. 3.16 and Eq. 3.18 is shown in Fig. 3.17. Further discussion about the relationship between the velocity distribution which is calculated by the curvature analysis and color distribution analysis will be the next step.

3.6. Conclusions

In conclusion, interference image analysis, that is, IFI method is proposed as a new method for the study of turbulence in 2D flowing soap films. In this method, only one image is needed to characterize the turbulence. It was calculated that the power spectrum of the interference pattern of soap films in the direction perpendicular to the mean flow direction (k_x direction) for different polymer concentrations. The power spectrum in the k_x direction included the information of polymer additives since the interference patterns became thin and long in the mean flow direction with PEO. This phenomena caused by the inhibition of the inverse transfers of energy, thus the vortices in the turbulence couldn't become large. The power component of the power spectrum in spatial frequency was in good agreement with the time frequency was obtained by LDV in previous work. It was extract that the exponent -5/3 for the thickness fluctuations of the turbulence in polymer free solution, and the exponents decreased toward -1 with polymer additives, which is also derived by theoretical work. The result of the Curvature analysis showed that the curvature histogram detects the variation of the vortices by PEO additives. The curvature of the interference pattern may correspond to the streamline, thus, the curvature histogram can be related to probability density function of the velocity fluctuation in the turbulence. The velocity fluctuation was also calculated by the color intensity distribution which is related to the thickness distribution. IFI methods will be useful as a simple and very low-cost solution for two-dimensional turbulence studies.

3.7. Reference

[1] R. H. Kraichnan, Inertial ranges in two-dimensional turbulence, *Phys. Fluids.* **10**, 1417 (1967)

[2] G. K. Batchelor, Computation of the energy spectrum in homogeneous two-dimensional turbulence, *Phys. Fluids. Suppl.* **II**, II-233 (1969)

[3] Y. Couder, Two-dimensional grid turbulence in a thin liquid film, *J. Phys. (France). Lett.* **45**, 353 (1984)

[4] Y. Couder, C. Basdevant, Experimental and numerical study of vortex couples in two-dimensional flows, *J. Fluid. Mech.* **173**, 225 (1986)

[5] M. Gharib, P. Derango, A liquid film (soap film) tunnel to study two-dimensional laminar and turbulent shear flows, *Physica. D.* **37**, 406 (1989)

[6] H. Kellay, X. L. Wu, W. I. Goldburg, Experiments with turbulent soap films, *Phys. Rev. Lett.* **74**, 3975 (1995)

[7] H. Kellay, X. L. Wu, W. I. Goldburg, Vorticity measurements in turbulent soap films, *Phys. Rev. Lett.* **80**, 277 (1998)

[8] H. Kellay, W. I. Goldburg, Two-dimensional turbulence: a review of some recent experiments, *Rep. Prog. Phys.* **65**, 845 (2002)

[9] H. Kellay, Polymers suppress the inverse transfers of energy and the enstrophy flux fluctuations in two-dimensional turbulence, *Phys. Rev. E.* **70**, 036310 (2004)

[10] A. Belmonte, W. I. Goldburg, H. Kellay, B. Martin, X. L. Wu, Velocity fluctuations in a turbulent soap film: The third moment in two dimensions, *Phys. Fluids.* **11**, 1196 (1999)

[11] B. K. Martin, X. L. Wu, W. I. Goldburg, M. A. Rutgers, Spectra of decaying turbulence in a soap film, *Phys. Rev. Lett.* **80**, 3964 (1998)

[12] M. A. Rutgers, Forced 2D turbulence: Experimental evidence of simultaneous inverse energy and forward enstrophy cascades, *Phys. Rev. Lett.* **81**, 2244 (1998)

[13] C. H. Bruneau, O. Greffier, H. Kellay, Numerical study of grid turbulence in two dimensions and comparison with experiments on turbulent soap films, *Phys. Rev. E.* **60**, R1162 (1999)

[14] C. H. Bruneau, H. Kellay, Experiments and direct numerical simulations of two-dimensional turbulence, *Phys. Rev. E.* **71**, 046305 (2005)

[15] O. Greffier, Y. Amarouchene, H. Kellay, Thickness Fluctuations in Turbulent Soap Films, *Phys.*

Rev. Lett. **88**, 194101 (2002)

[16] Y. Amarouchene, H. Kellay, Polymers in 2D turbulence: Suppression of large scale fluctuations, *Phys. Rev. Lett.* **89**, 104502 (2002)

[17] G. Boffetta, A. Celani, S. Musacchio, Two-dimensional turbulence of dilute polymer solutions, *Phys. Rev. Lett.* **91**, 034501 (2003)

[18] M. Rivera, P. Vorobieff, R. E. Ecke, Turbulence in Flowing Soap Films: Velocity, Vorticity, and Thickness Fields, *Phys. Rev. Lett.* **81**, 1417 (1998)

[19] P. Vorobieff, M. Rivera, R. E. Ecke, Soap film flows: statistics of two-dimensional turbulence, *Phys. Fluids.* **11**, 2167 (1999)

[20] M. K. Rivera, W. B. Daniel, S. Y. Chen, R. E. Ecke, Energy and enstrophy transfer in decaying two-dimensional turbulence, *Phys. Rev. Lett.* **90**, 104502 (2003)

[21] S. Chen, R. E. Ecke, G. L. Eyink, X. Wang, Z. Xiao, Physical mechanism of the two-dimensional enstrophy cascade, *Phys. Rev. Lett.* **91**, 214501 (2003)

[22] T. Shakeel, P. Vorobieff, Decaying turbulence in soap films: energy and enstrophy evolution, *Exp. Fluids.* **43**, 125 (2007)

[23] X. L. Wu, B. Martin, H. Kellay, W. I. Goldburg, Hydrodynamic convection in a two-dimensional couette cell, *Phys. Rev. Lett*. **75**, 236 (1995)

[24] Y. Amarouchene, H. Kellay, Batchelor Scaling in Fast-Flowing Soap Films, *Phys. Rev. Lett*. **93**, 214504 (2004)

[25] R. Hidema, Z. Yatabe, M. Shoji, C. Hashimoto, R. Pansu, G. Sagarzazu, H. Ushiki, Image analysis of thickness in flowing soap films. I: effects of polymer, *Exp. Fluids*, in press (2010)

[26] M. A. Rutgers, X. L. Wu, W. B, Daniel, Conducting fluid dynamics experiments with vertically falling soap films, *Rev. Sci. Instrum.* **72**, 3025 (2001)

[27] Z. Yatabe, Y. Miyake, M. Tachibana, C. Hashimoto, R. Pansu, H. Ushiki, Formation process of shear-induced onion structure made of quaternary system SDS/octanol/water/NaCl, *Chem. Phys. Lett.* **456**, 31 (2008)

[28] Z. Yatabe, R. Hidema, C. Hashimoto, R. B. Pansu, H. Ushiki, Size evolution of onion structure under oscillatory shear flow, *Chem. Phys. Lett.* **475**, 101 (2009)

[29] C. Hashimoto, J. Rouch, J. Lachaise, A. Graciaa, H. Ushiki, Complex macromolecular dynamics: I. Estimation technique for time-resolved emission anisotropy ratio of chromophores

incorporated into polymer chains, *Eur. Polym. J.* **40**, 1997 (2004)

[30] C. Hashimoto, P. Panizza, J. Rouch, H. Ushiki, Graphical analysis for gel morphology II. New mathematical approach for stretched exponential function with $\beta > 1$, *J. Phys. Condens. Mat.* **17**, 6319 (2005)

[31] C. Hashimoto, H. Ushiki, Graphical analysis for gel morphology. III. Gel size and temperature effects on the volume phase transition of gels, *J. Chem. Phys.* **124**, 044903 (2006)

[32] Y. Hattori, C. Hashimoto, J. Lashaise, A. Graciaa, H. Ushiki, Integral transformation method for sedimentation behaviours of aggregates Part I. a-Cyclodextrin/poly(ethyrene glycol)/water system, *Colloid. Surf. A.* **240**, 141 (2004)

[33] H. Ushiki, J. Rouch, J. Lachaise, A. Graciaa, Power law analysis of fluorescence decay curves of carbazolyl groups attached to polystyrene side chain, *Rep. Prog. Polym. Phys. Jpn.* **41**, 497 (1998)

Table 3.1. Fitting parameters of the distribution function (Eq. 3.16) for curvature histogram at various PEO concentrations.

Concentration (ppm)	A_1	γ	A_2
0	2.44×10^{1}	1.81	1.95×10^{2}
5	2.74×10^{1}	1.35	5.42×10^{1}
10	3.84×10^{1}	1.00	2.78×10^{1}
15	4.85×10^{1}	8.15×10^{-1}	1.96×10^{1}
20	9.28×10^{1}	5.10×10^{-1}	1.10×10^{1}
25	2.52×10^{2}	4.30×10^{-1}	1.24×10^{1}
30	1.39×10^{5}	1.38×10^{-1}	1.48×10^{1}

Table 3.2. Fitting parameters of the distribution function (Eq. 3.18) for color distribution at various PEO concentrations.

Concentration (ppm)	A_1	γ	A_2
0	1.23×10^{-2}	2.16	1.86×10^{3}
5	1.07×10^{-2}	2.13	1.36×10^{3}
10	1.10×10^{-2}	2.07	1.08×10^{3}
15	1.27×10^{-2}	1.95	8.13×10^{2}
20	1.30×10^{-2}	1.89	7.87×10^{2}
25	1.16×10^{-2}	1.77	4.55×10^{2}
30	1.51×10^{-2}	1.70	3.81×10^{2}

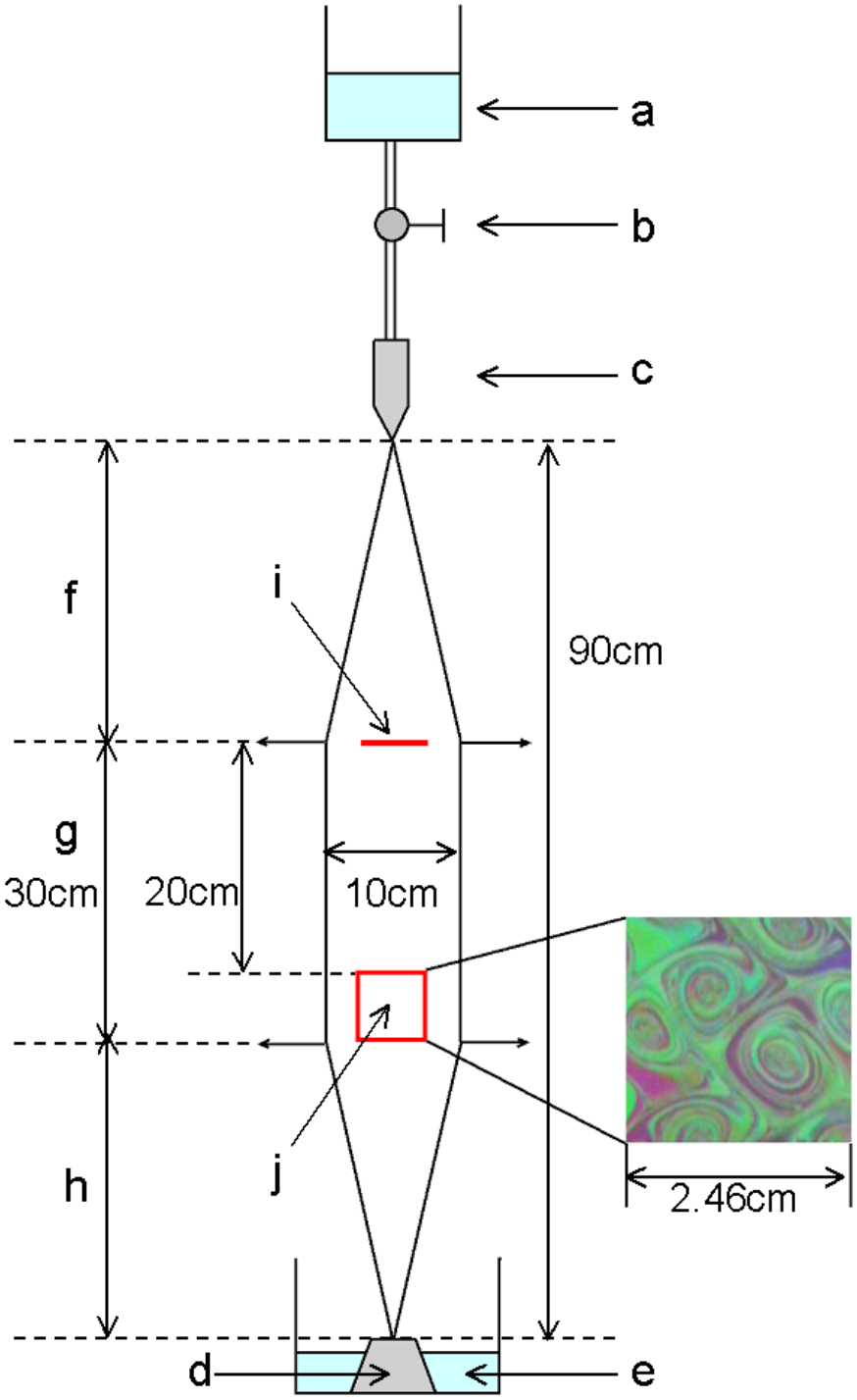

Figure 3.1. Schematics of the experimental setup (also see Rutgers 1999). (**a**) upper supply reservoir, (**b**) fluid metering valve, (**c**) nozzle, (**d**) tensioning weight, (**e**) bottom collection reservoir, (**f**) expanding section, (**g**) parallel section, (**h**) contracting section, (**i**) grid of cylindrical teeth, (**j**) data acquisition area.

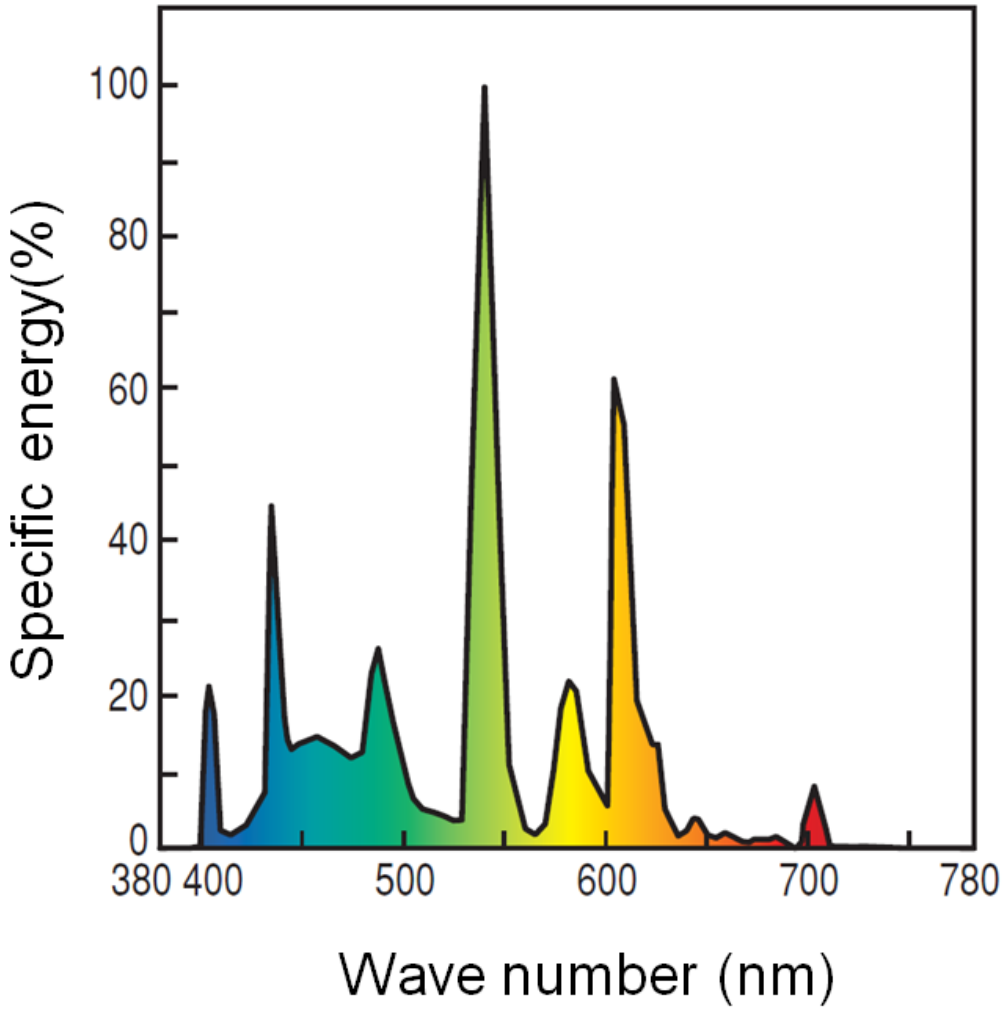

Figure 3.2. The data sheet provided by TOSHIBA Co. about the wave length of commercial white light source EFA25EN/22.

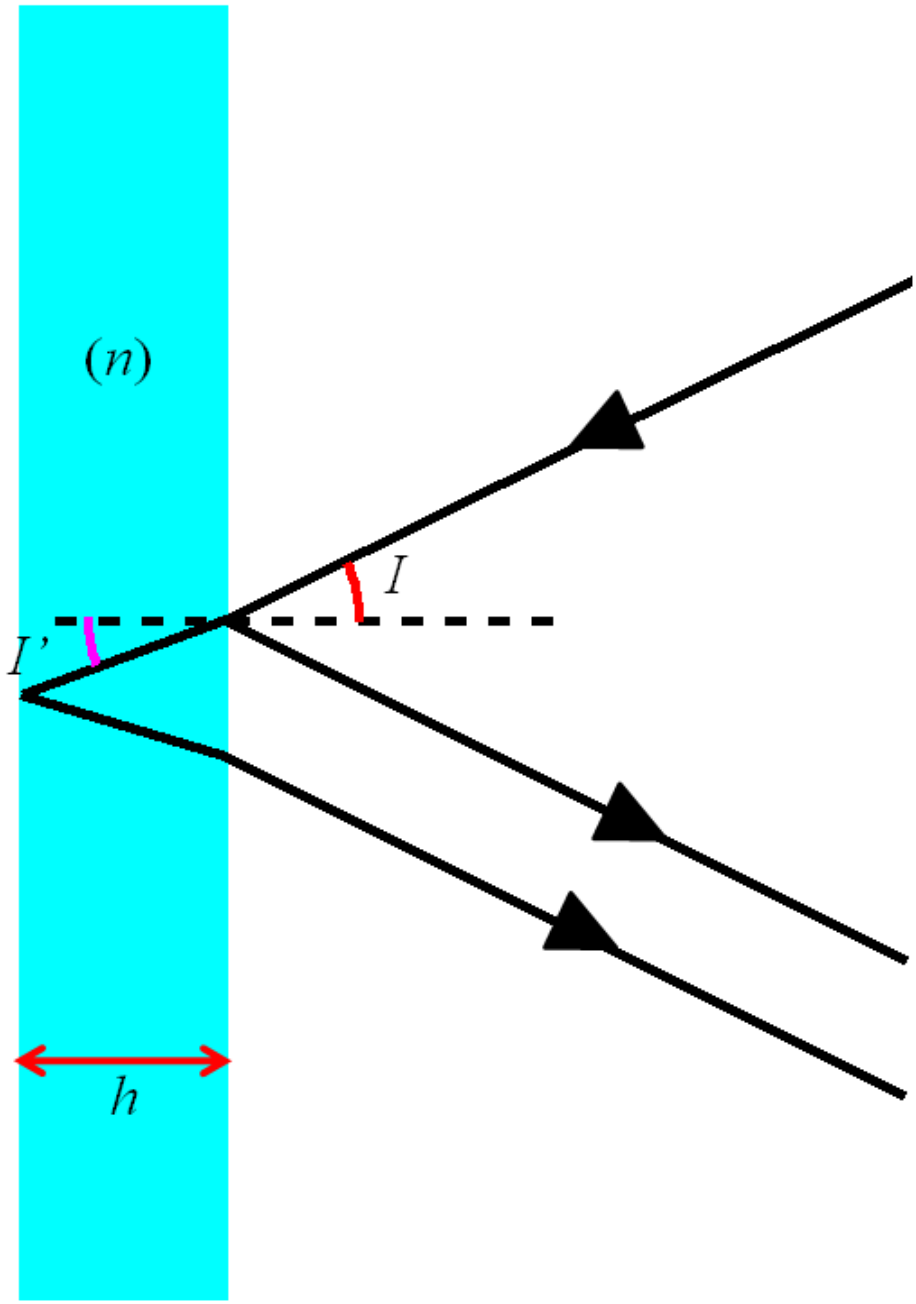

Figure 3.3. Schematic of the optical path of the illuminated light which is reflected on the soap film. The optical path is shown as black line, which is reflected on the front and back of the film. *n* is the refractive index in the water layer, *h* is the thickness of the film, and *I'* is the refraction angle at the back side of the film. In this experiment, n is 1.33 as water, d is 190nm, *cosI'* is assumed as 1.

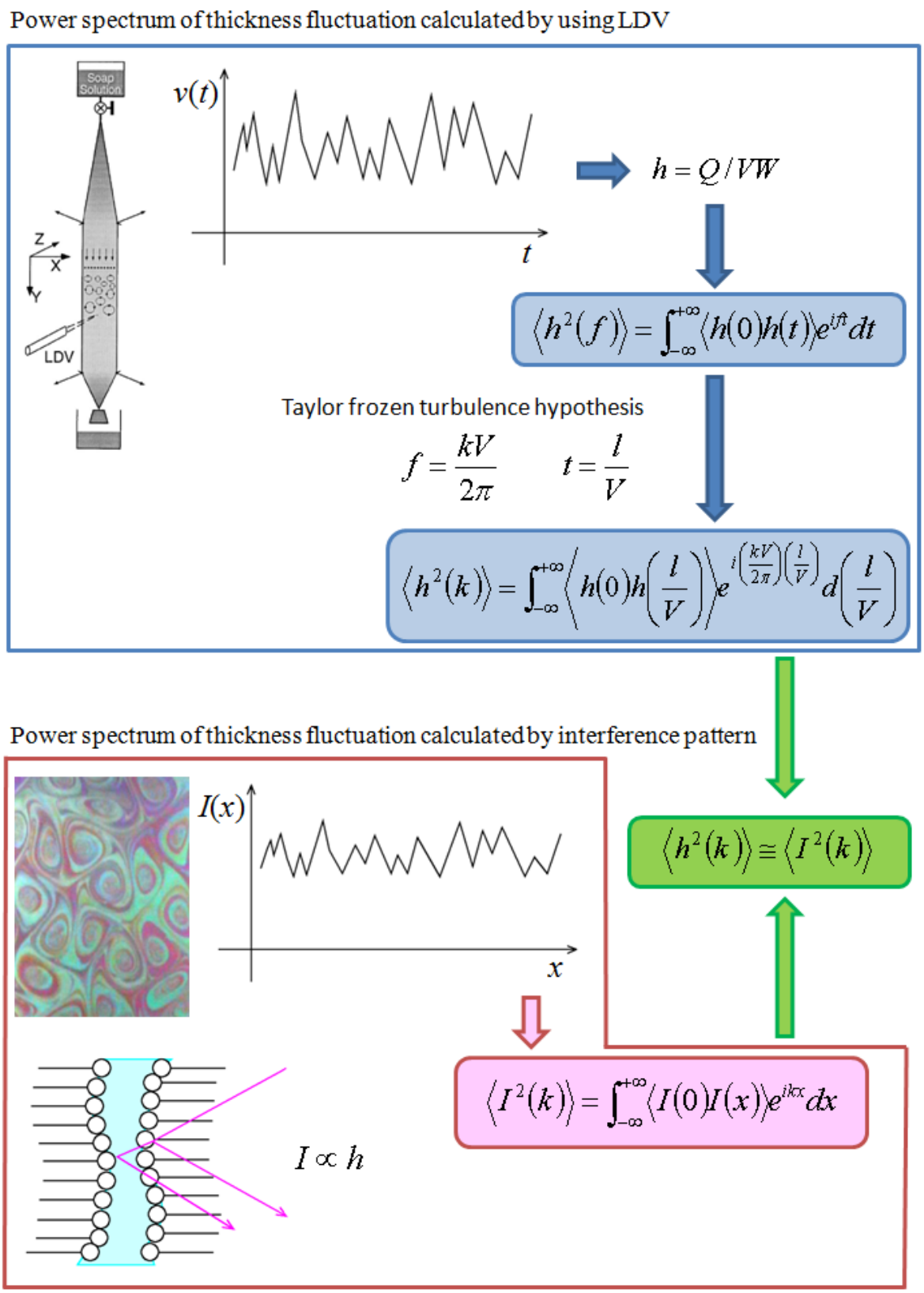

Figure 3.4. A schematic of the power spectrum of thickness fluctuation observed by using LDV and interference pattern.

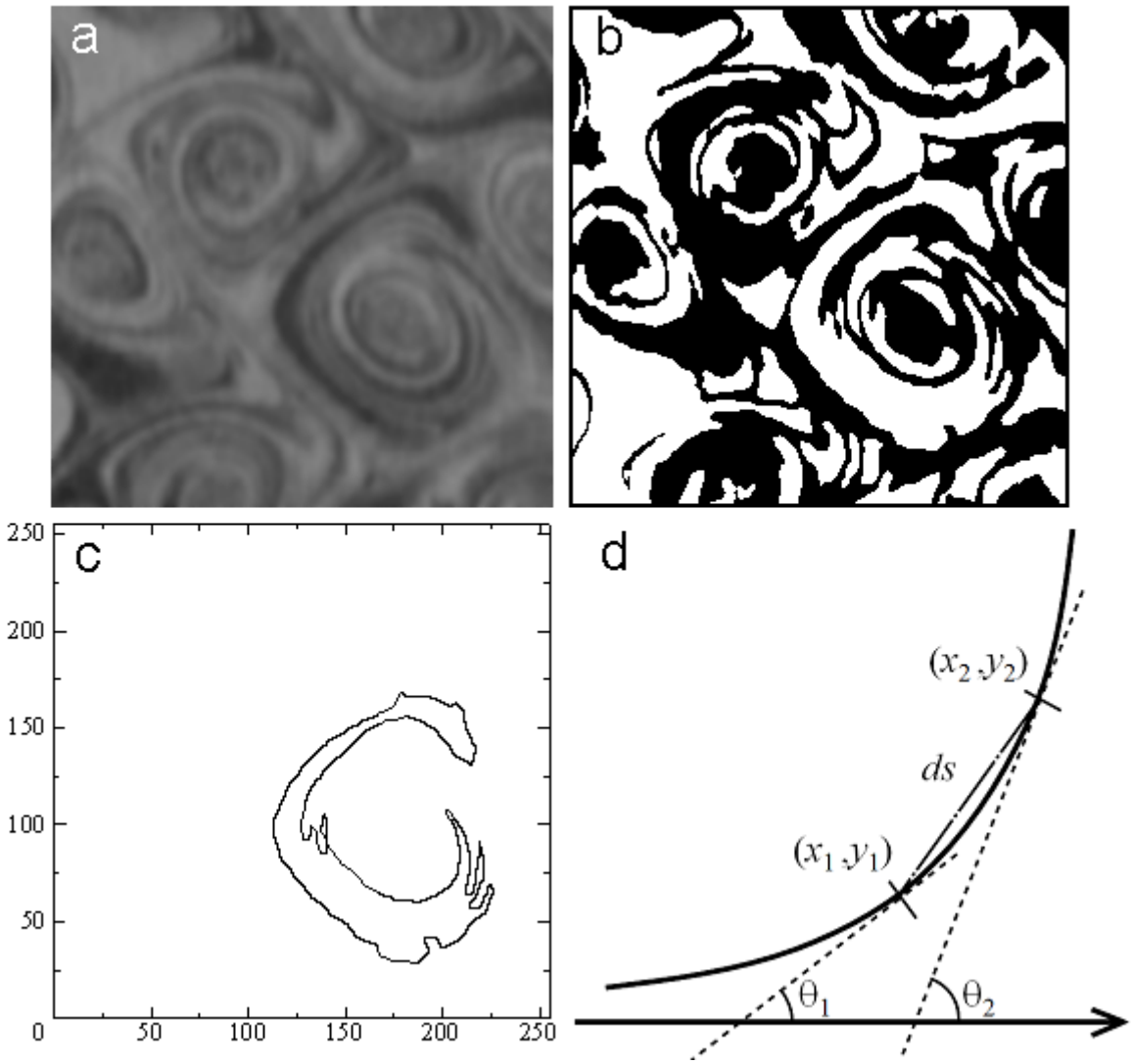

Figure 3.5. Schematic picture of the Curvature analysis software. (**a**) median filter image of intensity of color green; (**b**) black and white image of (**a**), (**c**) example of contour of one area in (**b**), (**d**) schematic picture for the calculation method of the curvature of the line.

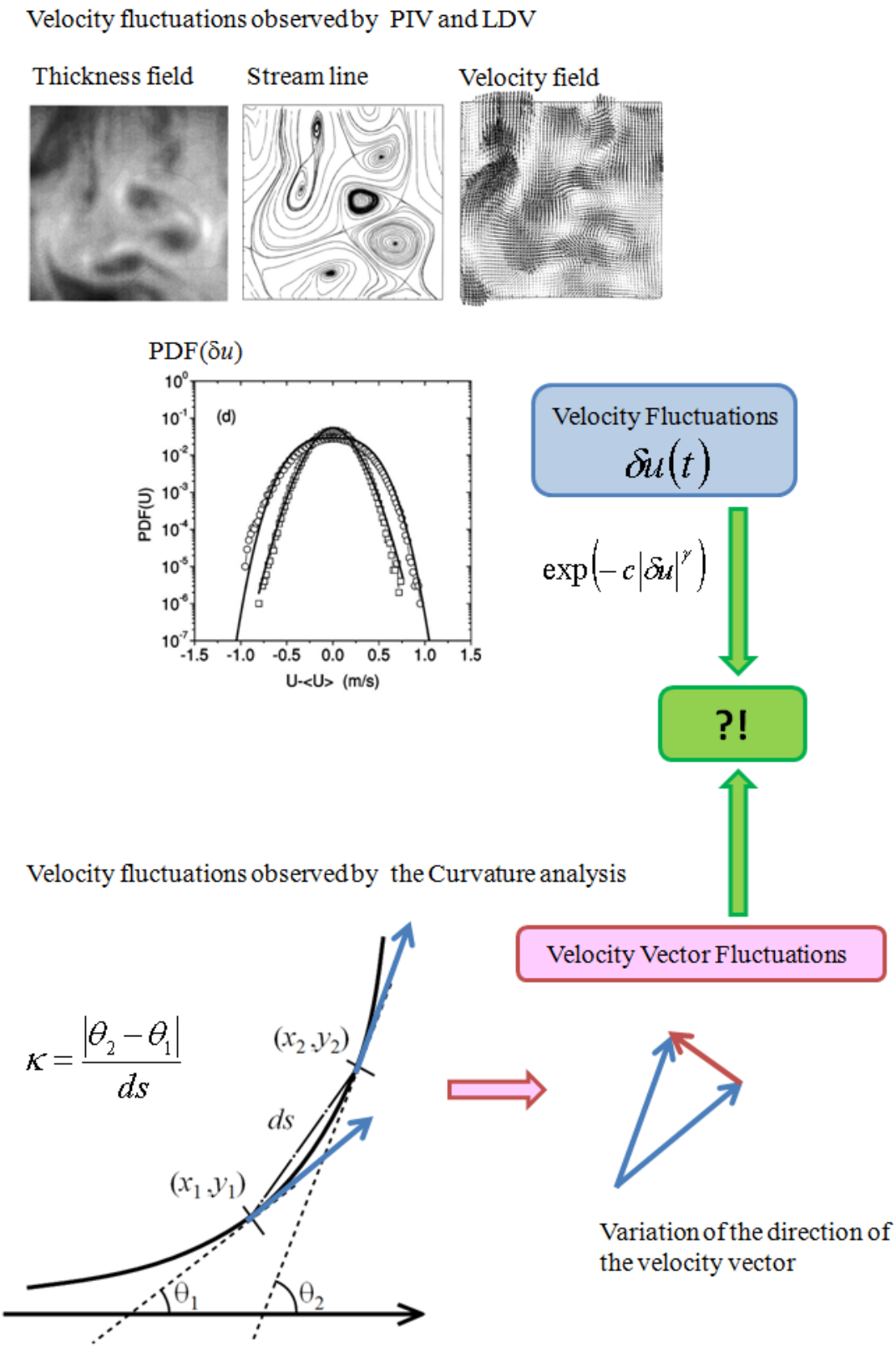

Figure 3.6. A schematic of the relationship between velocity fluctuation observed by LDV, PIV and Curvature analysis.

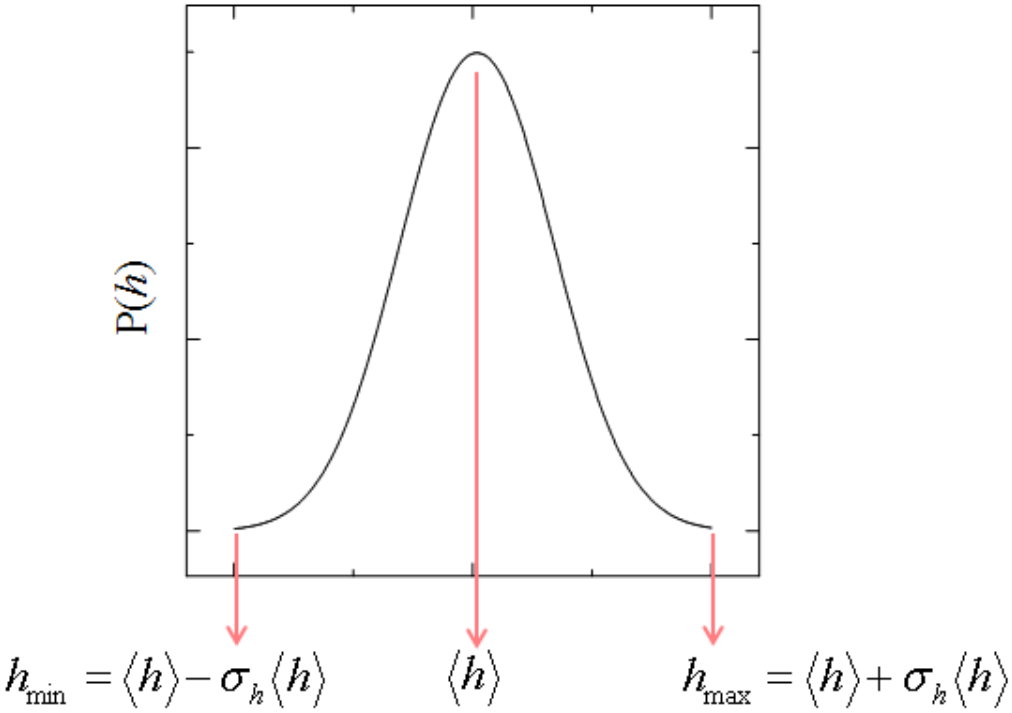

(a)

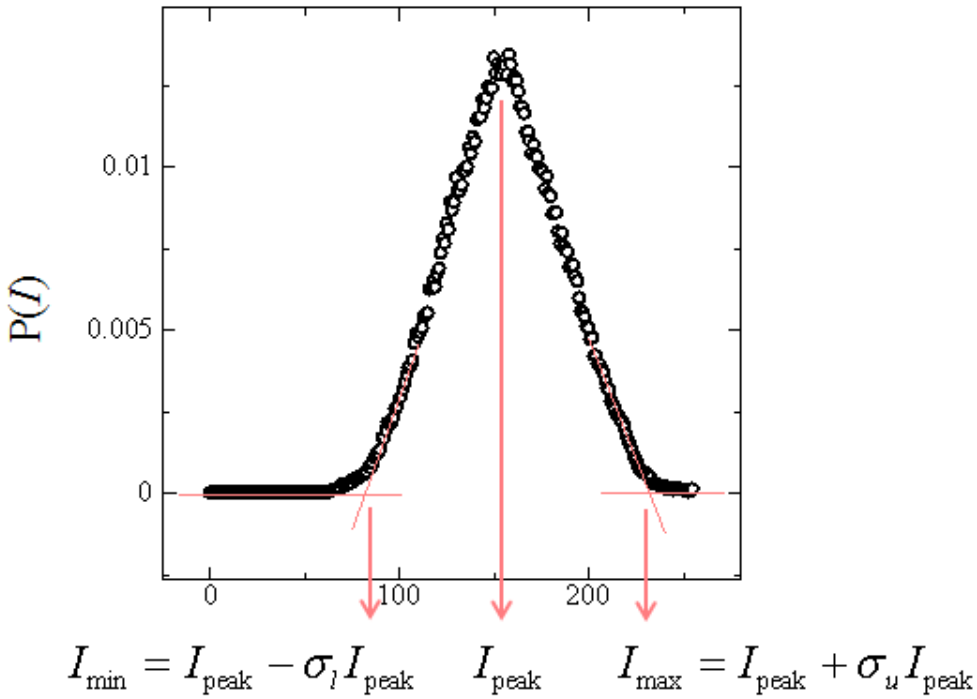

(b)

Figure 3.7. A schematic of the relationship between the thickness distribution and color intensity distribution.

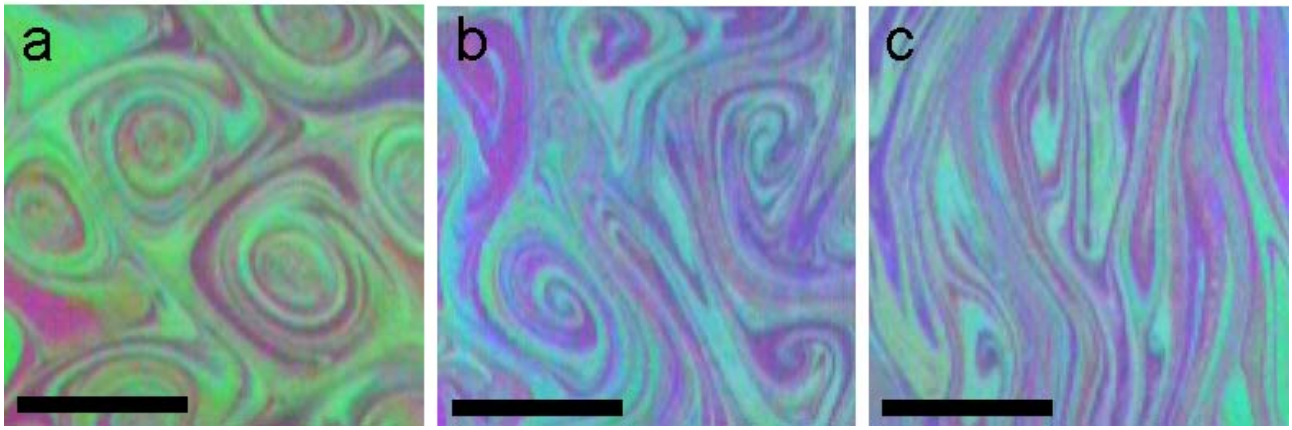

Figure 3.8. Two-dimensional grid turbulence in flowing soap films. The images are taken at (**a**) polymer free solution; (**b**) 15 ppm, (**c**) 30ppm PEO (4×10^6 molecular weight) solution for a mean velocity around 130 cm/s (see Sec.2.1 Experimental arrangement). Black bars indicate 1cm.

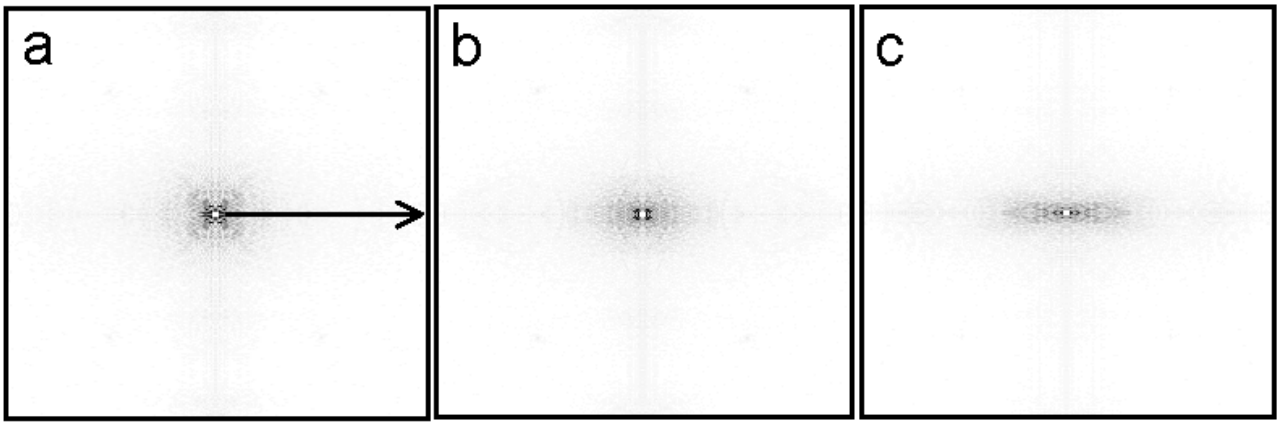

Figure 3.9. Two-dimensional representation of the power spectra, $<I_G^2(k)>$, of the turbulent images (see Fig. 3.7). The arrow direction in the image corresponds to the k_x direction.

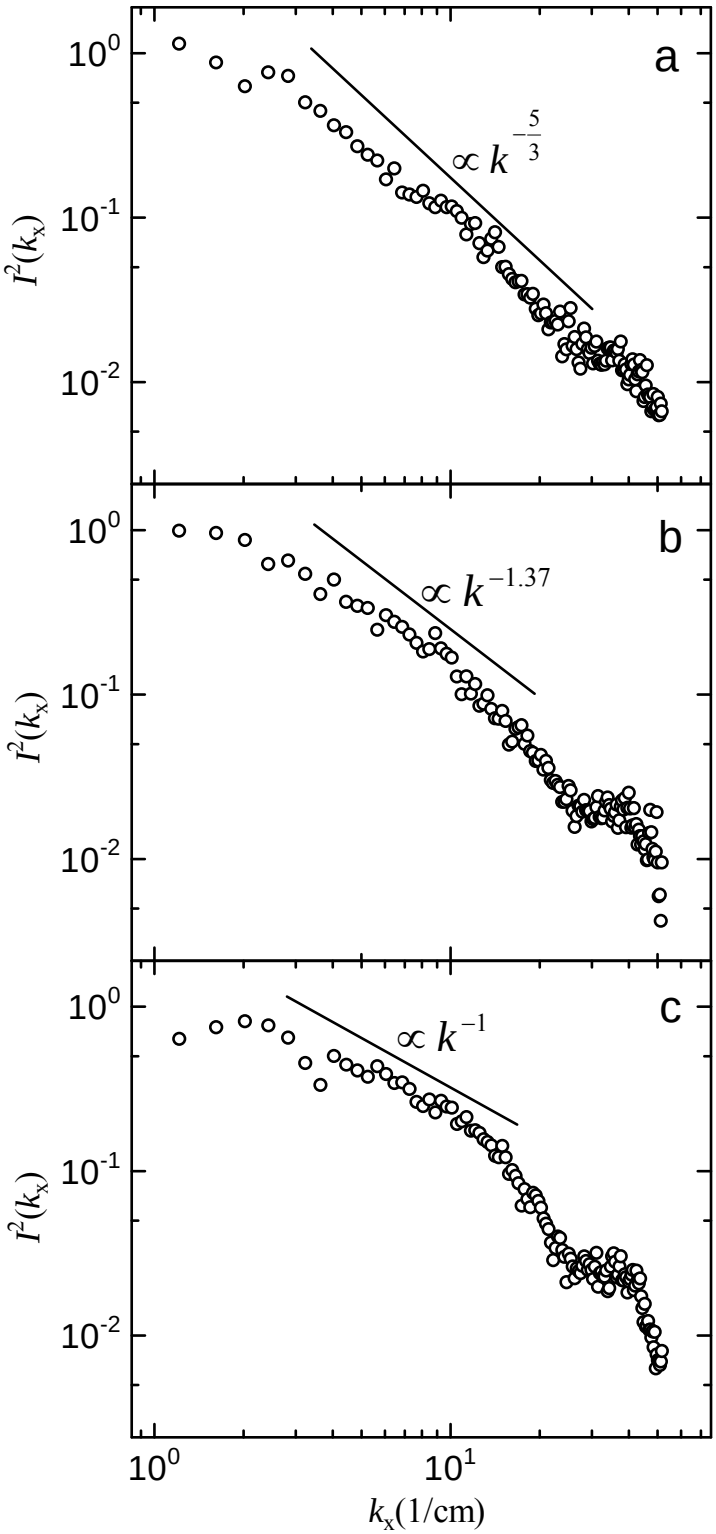

Figure 3.10. Scaling form of the spectral density $<I_G^2(k)>$ along the arrow direction (see Fig. 4) for different polymer concentrations (**a**) polymer free solution; (**b**) 15 ppm, (**c**) 30ppm PEO solution (4×10^6 molecular weight). The solid line with a slope of –5/3, –1.37 and –1 are calculated by fitting.

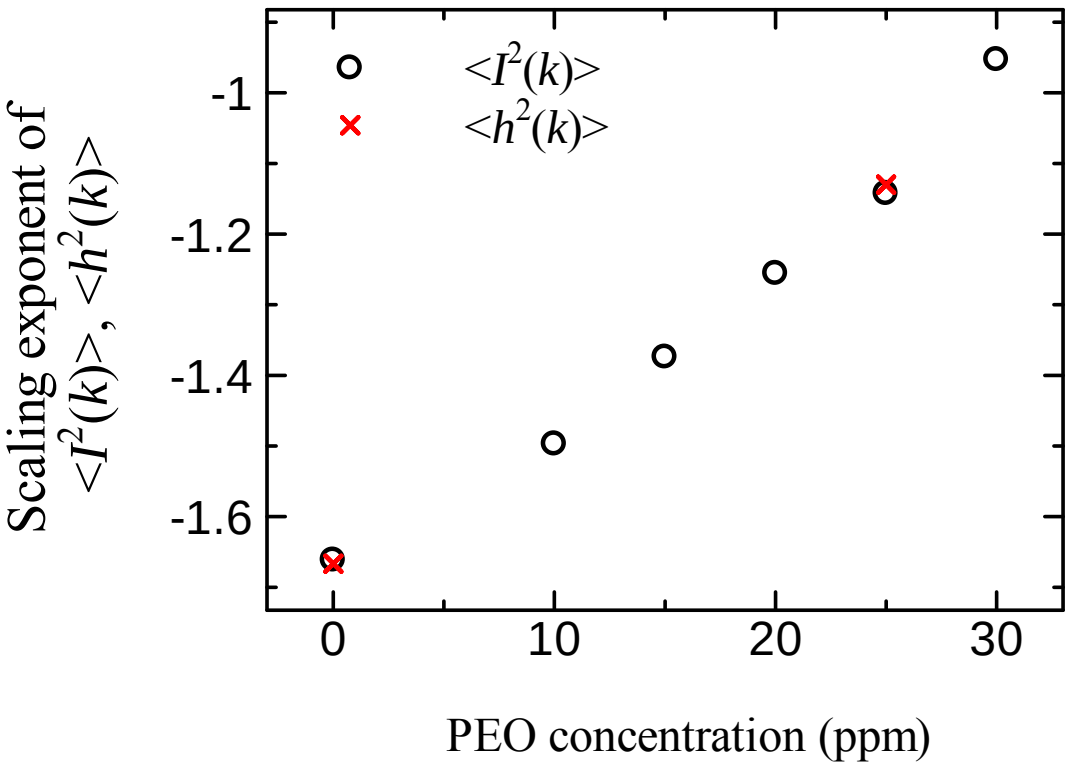

Figure 3.11. Comparison of the value of scaling exponent obtained by LDV observation [16] and 2D Fourier analysis.

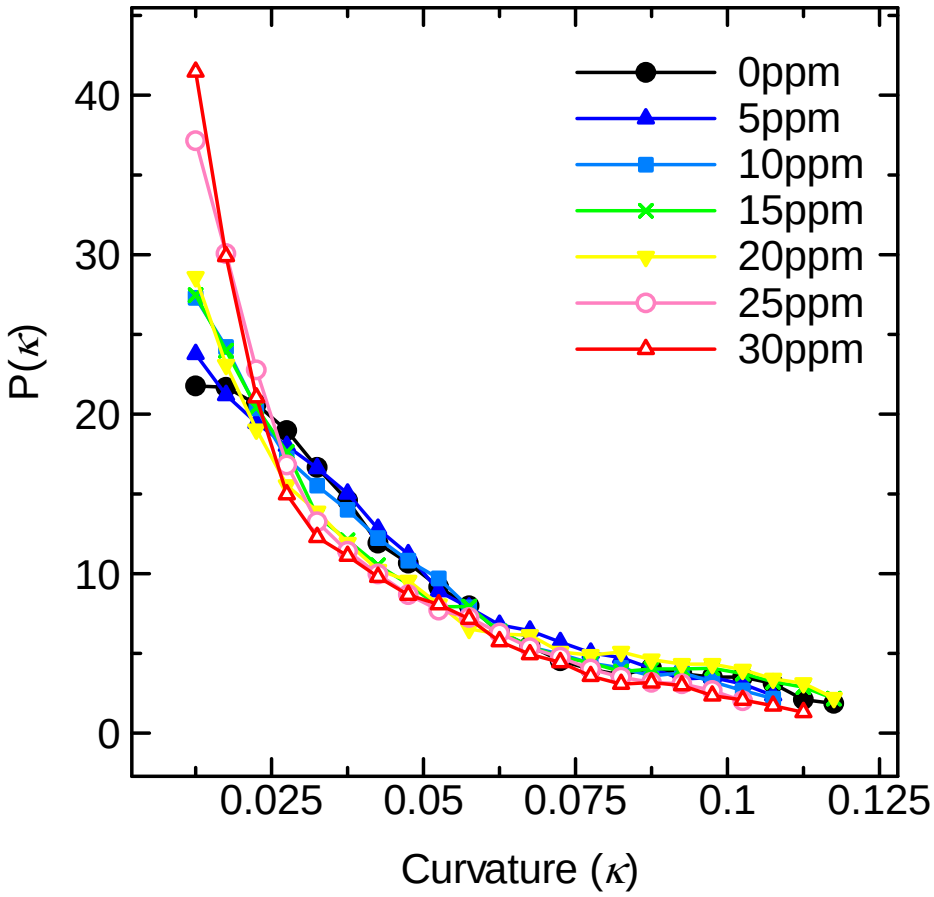

Figure 3.12. Curvature histogram for different polymer concentrations as indicated in ppm.

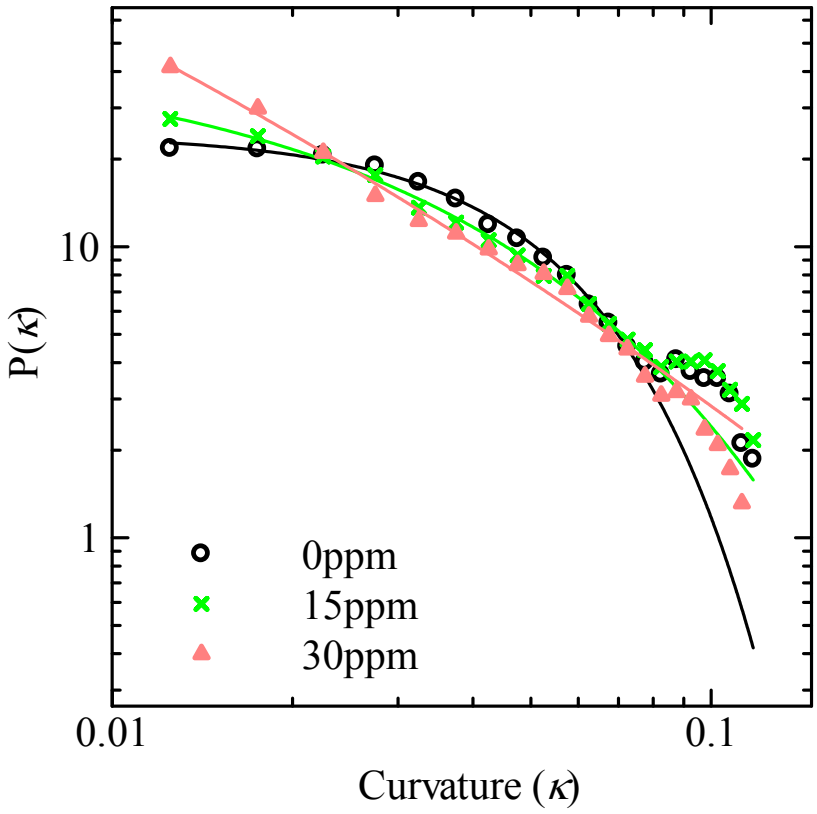

Figure 3.13. Curvature histogram for different polymer concentrations. The solid lines are the best fit probability density function (Eq. 3.16) for each histogram of different polymer concentration, PEO solution (4×10^6 molecular weight).

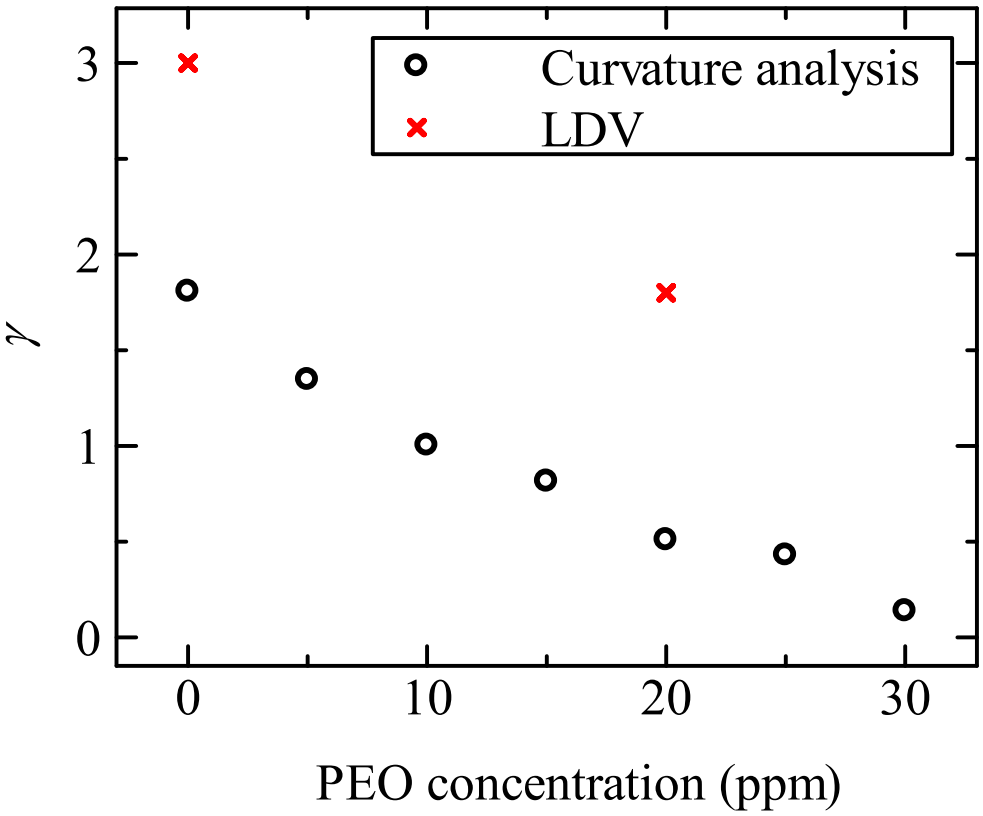

Figure 3.14. Comparison of the value of the fitting parameter γ obtained by LDV observation [9] and Curvature analysis.

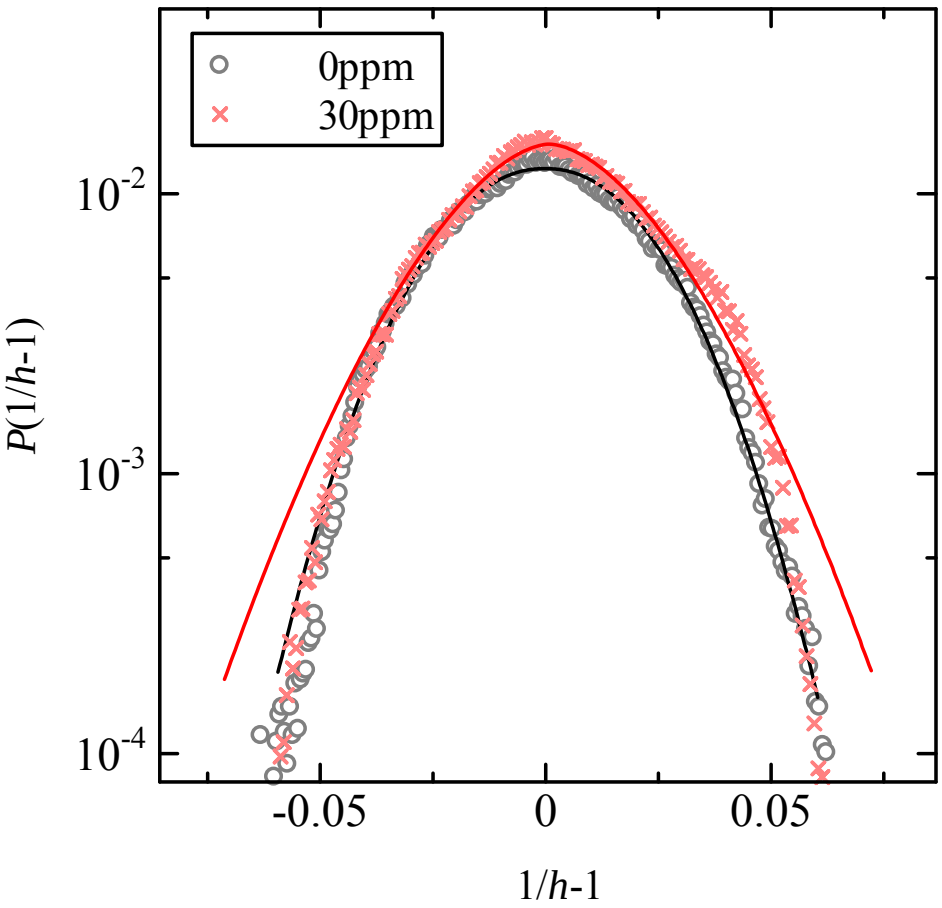

Figure 3.15. Histogram of $1/h$-1. The solid lines are the best fit probability density function (Eq. 3.18) for each histogram of different polymer concentration, PEO solution (4×10^6 molecular weight).

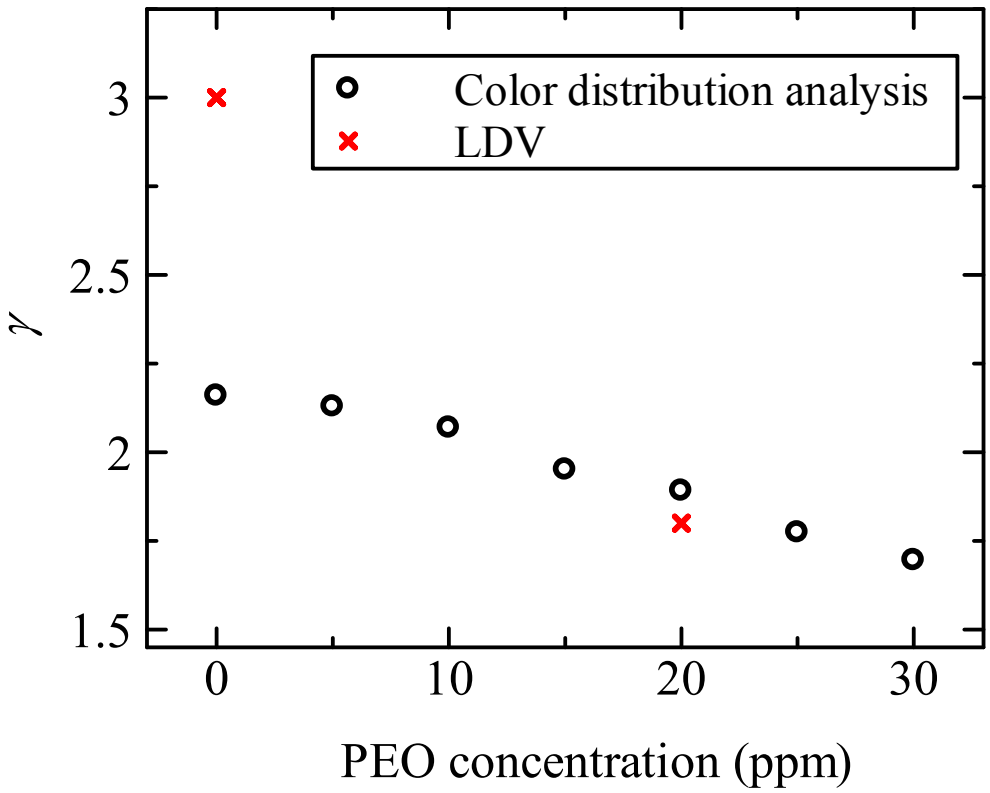

Figure 3.16. Comparison of the value of the fitting parameter γ obtained by LDV observation [9] and color distribution analysis.

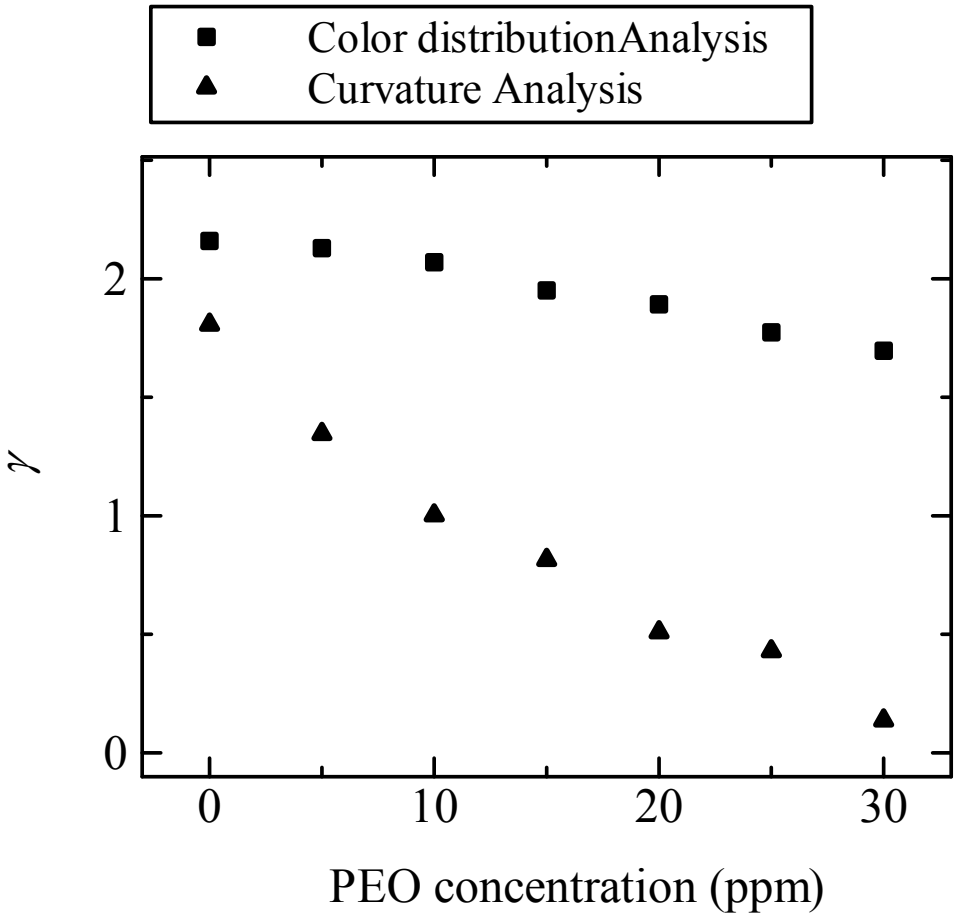

Figure 3.17. Comparison of the value of the fitting parameter γ obtained by curvature analysis and color distribution analysis.

Chapter 4

General Conclusion

In this thesis, the original way of single-image analysis as a new ideas and technique is proposed to quantify the turbulence. Since turbulence is very complicated, discussions of the turbulence have a tendency to treat fussy details. Thus, an attempt was made to analyze the turbulence by image analysis. The turbulence in flowing soap films as a 2D turbulence was chosen in order to visualize the 2D flow easily by observing the interference pattern of the soap film. The new image analysis method is named as IFI method, since the method analyze the turbulence by the *interference image* of the soap film. Besides, the effects of polymer on the 2D turbulence were also quantified by IFI method. To detect and quantify the polymer effects in turbulence is the long standing issue, thus, very simple way like a IFI method will useful way to observe and investigate the phenomena.

In chapter 2, previous studies of 2D turbulence are summarized as a background of this thesis. In the first stage of the 2D flow researches, the single-point measurement using a LDV and the scaling law analysis was only the technique to measure the turbulence. The scaling exponent was only the way to detect the variation of inverse energy cascade and enstrophy cascade in the 2D flow, which was affected by polymer additives. The distributions of the velocity fluctuations were also detected, which became narrower by additives. In order to see the *flow field*, two-points measurement using two LDV apparatuses, and PIV method have been developed. However, the single-image analysis by the way of image processing of 2D flow was quite rare, even the interference pattern of the soap film as a 2D flow shows the *flow field* directly by reflecting the light.

In chapter 3, we proposed the IFI method to analyze turbulence using flowing soap films. Since the interference pattern is related to the thickness, the patterns show the information of the flow. The power spectrum of the interference patterns were calculated, indeed the scaling exponent of the power spectrum in spatial frequency was consistent with that of the thickness fluctuation in time frequency calculated by LDV analysis, which was also derived by theoretical work. The curvature histogram of the interference pattern was calculated. The interference pattern is related to the thickness, furthermore the vorticity and the streamlines. That is why the curvature of the interference patterns can be related to the velocity fluctuations. Thus, the distribution which was related to the velocity fluctuations of the turbulence could be detected by the curvature histogram. The velocity fluctuations were also calculated by the intensity distribution of the interference image.

Besides, the IFI method could detect well the variation of the turbulence by polyethylene oxide additives.

In conclusion, 2D turbulence and effect of polymer on the turbulence are quantified by IFI method. The turbulence was visualized and quantified clearly with this method, which let the turbulence researches much simpler. Thus this method will give new approach to the drag reduction and other complex fluids. Besides, flowing soap films as a 2D flow includes not only the fundamental problem of fluid dynamics but also the confined space which was made by surfactant bilayer. Indeed, such a situation can be seen in nature such as cell membrane and synovial fluid. IFI method has possibilities to analyze any turbulent flow from large scale such as metrological phenomena to small scale such as cell membrane or synovial fluid.

Acknowledgment

I would like to inscribe cordial acknowledgment to who support these studies.

First of all, I express my appreciation to Professor USHIKI Hideharu at Tokyo University of Agriculture and Technology. He gave me a chance to make these researches in Japan, and also gave me a chance to study in France. Through the daily life discussion with him, I could have strong motivation for these researches and consider to my life as a researcher.

For the committee of this thesis, I express gratitude cordially to Professor TAKAYANAGI Masao at Tokyo University of Agriculture and Technology, Professor YONEKURA Masami at Ibaraki University, Professor UDA Yasushi at Utsunomiya University and Professor FUNADA Ryo at Tokyo University of Agriculture and Technology.

I wish to thank cordially to Dr. YATABE Zenji, Professor SHOJI Masahiko and Professor HASHIMOTO Chihiro for their help and fruitful discussion. I also appreciate to share the time in my younger days with them, which let me consider and feel many things.

I am grateful to Professor FURUKAWA Hidemitsu at Yamagata University. I really appreciate his fruitful comments for this work, and ideas for many topics of fundamental natural science.

I am grateful to Professor PANSU Robert at ENS-Cachan for providing me the opportunity to make studies and taking care of my stay in France as a student of the Collège doctoral franco-japonais.

I wish to thank cordially to Ms. RALEA Adina and Ms. POCOVNICU Oana for their friendship and giving me many aspects to consider our life. I am proud and feel happy to meet you in France and to discuss many things as a citizen of the world. Our friendship will be forever.

I also thank to all the members in USHIKI laboratory. Thanks to them, I could have opportunity to consider many things and to share many experiences.

Finally, I would like to thank to my mother and my fiancé Dr. SAGARZAZU Gabriel for their continuously, generous and maximum support and love for my life and study.

11 July, 2010

Ruri HIDEMA
United Graduate school of Agricultural Science,
Tokyo University of Agriculture and Technology.
3- 5- 8 Saiwai - cho, Fuchu, Tokyo 183- 8509, Japan